

# Radio Astronomy Project

## WP100 Receiver Characterisation

### Final Report



**Projekt Amateurfunk at the Chair of High Frequency Technology and  
Project Satellite Communication at the Chair of Space Technology of TU Berlin**

Assessors: Prof. Dr.-Ing. Maurizio Burla, Sebastian Lange

Advisors: M.Sc., Camille Westerhof, Anna Engler, Timo Samuel Prinz, Martin Hübner

Authors: Leo Müller, Daniel Schreiber

Summer Semester 2025

Turned in on August 28, 2025

## Contacts

Technische Universität Berlin  
Institut für Hochfrequenz- und Halbleiter-Systemtechnologien  
Fachgebiet Hochfrequenztechnik-Photonik  
Fakultät IV

Einsteinufer 25  
10587 Berlin  
Deutschland

Phone: +49 (0)30 314 22 637  
Fax +49 (0)30 314 24 626

[www.hft.tu-berlin.de](http://www.hft.tu-berlin.de)

and

Technische Universität Berlin  
Institut für Luft- und Raumfahrt  
Fachgebiet Raumfahrttechnik  
Fakultät V

Marchstraße 12 - 14  
10587 Berlin  
Deutschland

Phone: +49 (0)30 314 21 305  
Fax: +49 (0)30 314 21 306

[www.rft.tu-berlin.de](http://www.rft.tu-berlin.de)

## Team

**Project Manager** Daniel Schreiber

**Team Members** Leo Müller

Revised on August 26, 2025

## Abstract

This report investigates the suitability of various low-cost software-defined radios for use in a microwave radiometer for measuring thermal radiation. The focus lies on key parameters such as gain drift, noise figure, dynamic range, and integration time. The PlutoSDR shows the most stable and consistent performance overall. The RTL-SDR exhibits significant fluctuations but remains of interest due to its low cost. A comprehensive evaluation of the SDR measurement results still requires characterization of the LNB.

## List of Abbreviations

- **BALUN** Balanced Unbalanced
- **dB** Decibel
- **ENR** Excess Noise Ratio
- **GPIB** General Purpose Interface Bus
- **IF** Intermediate Frequency
- **LNA** Low Noise Amplifier
- **LNB** Low Noise Block Downconverter
- **LO Frequency** Local Oscillator frequency
- **RBW** Resolution Bandwidth
- **SDR** Software Defined Radio
- **DR** Dynamic Range in dB
- **ENOB** Equivalent Number of Bits
- **RX / DRX Port** Receiver / Diversity Receiver Port

# Contents

Contacts . . . . .	2
Abstract . . . . .	3
List of Abbreviations . . . . .	4
<b>1 Introduction</b>	<b>7</b>
<b>2 Theory</b>	<b>8</b>
2.1 Receiver Chain Setup . . . . .	8
2.2 Noise Temperature . . . . .	8
2.3 Sensitivity of the receiver . . . . .	9
2.3.1 Equivalent Number of Bits (ENOB) . . . . .	9
2.3.2 Noise Figure . . . . .	9
2.3.3 Integration Time . . . . .	11
2.3.4 Gain Drift . . . . .	11
2.4 Bandwidth . . . . .	12
2.5 Radio Quiet Zone . . . . .	12
2.6 SDR internal signal chain . . . . .	12
<b>3 General Experimental Setups and Procedures</b>	<b>13</b>
3.1 Laboratory equipment used . . . . .	13
3.2 Used SDRs . . . . .	13
3.3 General Settings GNU Radio Signal Processing Chain . . . . .	14
3.4 Automation . . . . .	15
3.4.1 GPIB . . . . .	15
3.4.2 Python embedding . . . . .	17
3.5 Repository . . . . .	17
<b>4 Calibration of the Signal Generator</b>	<b>18</b>
4.1 Set Up . . . . .	18
4.2 Results . . . . .	20
<b>5 Dynamic Range</b>	<b>22</b>
5.1 Set Up . . . . .	22
5.2 Estimation of SDR Input Power . . . . .	24
5.3 Results . . . . .	24
5.3.1 Pluto SDR . . . . .	26
5.3.2 RTL-SDR . . . . .	26
5.3.3 HackRF SDR . . . . .	27
5.3.4 USRP B210 . . . . .	27

5.3.5 USRP B200 Mini . . . . .	28
<b>6 Gain Drift</b>	<b>30</b>
6.1 Setup . . . . .	30
6.2 Results . . . . .	31
6.3 Drift at expected Radiometric Input Power . . . . .	34
6.4 Temperature Dependence . . . . .	34
6.5 Estimation of Receiver Sensitivity . . . . .	35
6.6 Improvement of Investigation . . . . .	35
<b>7 Integration Time</b>	<b>36</b>
7.1 Set Up . . . . .	36
7.1.1 Initial Approach and Lessons Learned . . . . .	37
7.2 Results . . . . .	38
<b>8 Noise Figure</b>	<b>41</b>
8.1 Set Up . . . . .	41
8.2 Results . . . . .	42
8.2.1 Noise Figure in complete Receiver Chain . . . . .	45
<b>9 Conclusion</b>	<b>46</b>
9.1 Usage Recommendation . . . . .	46
9.2 Future Investigations . . . . .	46
<b>10 List of Figures</b>	<b>48</b>
<b>11 Bibliography</b>	<b>51</b>
<b>12 Appendix</b>	<b>53</b>
12.1 Setup Photos . . . . .	53
12.2 Estimation of SDR Input Power . . . . .	60
12.3 Dynamic Range Results . . . . .	61
12.3.1 Dynamic Range Plots . . . . .	61
12.3.2 Dynamic Range Tables . . . . .	70
12.4 Gain Drift . . . . .	72
12.4.1 Estimation of Receiver Sensitivity . . . . .	72
12.5 Integration Time . . . . .	73
<b>13 Affidavit of Independent Work and Declaration of AI Use</b>	<b>78</b>

# 1 Introduction

Since ancient times, humanity has been fascinated by the stars and driven by a desire to understand the universe beyond our own planet. Radio astronomy enables the measurement of thermal radiation emitted by celestial bodies and thus provides valuable insights into their physical properties, particularly their temperature. While professional radio telescopes offer high precision, they are typically associated with high costs and considerable technical complexity. Consequently, there is growing interest in low-cost alternatives that are still capable of delivering sufficiently accurate measurements.

As part of the course "Radio Astronomy" led by Prof. Dr.-Ing. Burla at the Chair of High-Frequency Engineering at TU Berlin, the goal is to develop a low-cost radiometer. The aim of the project is to detect thermal radiation from celestial bodies, in particular the Sun, using a parabolic dish antenna and to derive its temperature. This concept builds on the work of Schiavolini et al. [15], in which a low-cost microwave radiometer was implemented using a low-noise downconverter originally intended for satellite TV reception and a software-defined radio. The overall project is divided into several parallel working groups that address topics such as the characterization of the receiver chain, the development of a calibration method, software implementation, and mechanical construction.

This technical report documents Workpackage 100, which focuses on the characterization of the receiver chain. The chain consists of a Bullseye LNB that receives thermal noise around 10 GHz and downconverts the signal to an intermediate frequency near 1 GHz, where it is then processed by an SDR.

Although SDRs and LNBs are well-established in industrial applications, radiometric use cases require different performance parameters than typical communication applications. Schiavolini et al. have already evaluated dynamic range, noise figure, and integration time for the RTL-SDR [4]. In this report, the evaluation is extended to include the PlutoSDR[6], HackRF[7], USRP B200[5], and USRP B210[5], with additional measurements of gain drift for each SDR.

To ensure reproducibility, the entire measurement process was automated using Python, integrating GNU Radio signal chains, data evaluation, and device control. All implementations were consolidated in a central repository.

The primary objective of this work is to identify the differences between the investigated SDRs with respect to their suitability for radiometric applications and to provide a usage recommendation. Given the substantial price differences between the devices, this evaluation is not only technically relevant but also economically significant. Professional laboratory equipment was used to obtain reliable reference values, which may also serve in other application contexts.

A special thanks goes to Camille Westerhof, who supported us throughout the project as our advisor and significantly contributed to the success of this work.

## 2 Theory

The goal of radio astronomy is to measure thermal radiation from celestial objects such as the sun by directing an antenna towards the source. In contrast to conventional radio transmissions that rely on a carrier frequency, thermal radiation appears as broadband continuous noise across the spectrum, whose intensity can be expressed as an equivalent temperature<sup>1</sup>. However, the equipment must fulfill different requirements compared to traditional television reception, as described in the following sections.

### 2.1 Receiver Chain Setup

The radiometer consists of a parabolic dish with an LNB. Its output is then fed into an SDR, a novel approach, since little calibration has been done in this field so far.

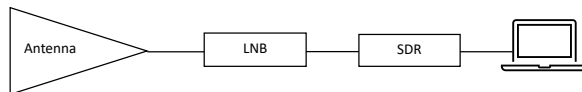


**Figure 2.1:** Receiver Chain

### 2.2 Noise Temperature

Due to temperature inequalities that occur at temperatures greater  $T = 0$  K, spontaneous movement of electrons causes thermal noise in a system. Its power is calculated by 2.1, where  $k_B$  is the Boltzmann Constant,  $B$  the bandwidth over which the noise is measured and  $T$  the temperature.

$$P_{Th} = k_B T B \quad (2.1)$$

For a known noise power and Bandwidth we can also retrieve an apparent Noise Temperature, which might not represent the actual physical temperature of the noisy source but a temperature of a resistor that would produce the same noise power.

---

<sup>1</sup>For low frequencies, as in our case, black body radiation is approximately constant across the frequency band

## 2.3 Sensitivity of the receiver

The sensitivity  $\Delta T_{min}$ , of a radiometric receiver is given by 2.2 [17]. It describes the smallest change in Noise Temperature that can be detected.

$$\Delta T_{min} = T_{SN} \sqrt{\left(\frac{1}{B_{HF}\tau_I}\right)^2 + \left(\frac{\Delta G}{G_0}\right)^2} \quad (2.2)$$

The sensitivity depends on the following metrics characterizing a receiver:

### 2.3.1 Equivalent Number of Bits (ENOB)

The ENOB indicates the number of bits an ideal analog-to-digital converter (ADC) would need to achieve the same dynamic range as the actual ADC. Nonlinearities and other imperfections can limit the effective resolution. With eq. (2.3) an estimate of the effective number of bits based on the measured dynamic range can be calculated.

$$ENOB = \frac{DR - 1,76 \text{ dB}}{6,02 \text{ dB}} \quad (2.3)$$

### 2.3.2 Noise Figure

In 2.2  $T_{SN}$  describes the system noise temperature, composed of the, to be measured, antenna noise temperature  $T_A$  and the receiver noise temperature  $T_R$ .

$$T_{SN} = T_A + T_R \quad (2.4)$$

The latter describes the added noise by the receiver and can be also expressed by the equivalent Noise Figure  $F_R$  2.5.

$$T_R = (F_R - 1)T_0 \quad (2.5)$$

The Noise Figure describes the degradation of the Signal to Noise Ratio in a system 2.6.

$$F = \frac{SNR_{out}}{SNR_{in}} \quad (2.6)$$

### Cascaded Systems

In cascaded systems 2.2 where every stage is given by a Gain  $G_i$  and a Noise Figure  $F_i$ , the complete Noise Figure calculates by Friis Formula 2.7, which shows that the first stage has the biggest impact since the following are decreased by the gain of the previous stages.

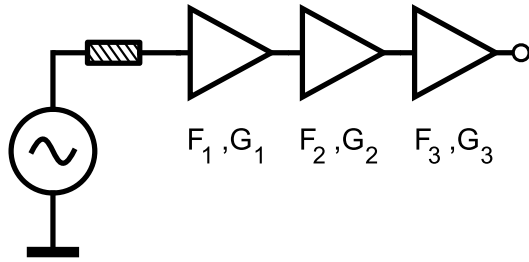


**Figure 2.2:** Cascaded system with Gain and Noise Figure per stage [10]

$$F_{total} = F_1 + \frac{F_2 - 1}{G_1} + \frac{F_3 - 1}{G_1 G_2} + \frac{F_4 - 1}{G_1 G_2 G_3} \quad (2.7)$$

### Y-Factor Method

To measure the Noise Figure of a device, the Y-Factor method is used as a calibrated noise source is available.



**Figure 2.3:** calibrated noise source

If turned off only thermal noise at room temperature is measured ( $N_C$ ) and if supplied with 28V a different noise power is measured ( $N_H$ ). The two measured powers can be used to calculate the Y Factor eq. (2.8) and with that the device noise figure eq. (2.9).

$$Y = \frac{N_H}{N_C} \quad (2.8)$$

$$F \approx \frac{ENR}{Y - 1} \quad (2.9)$$

$$(2.10)$$

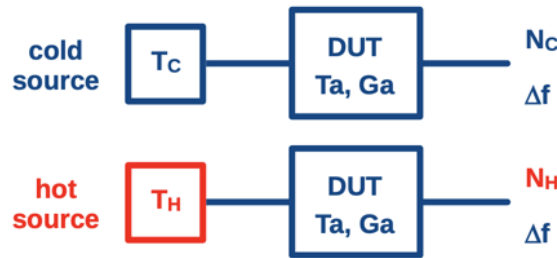


**Figure 2.4:** Y-Factor method hot and cold source measurement [1]

This method only works when operating in a linear region of the device. To later check this, the input power of the noise source is calculated at a bandwidth of 2MHz as shown in eq. (2.11) and eq. (2.13).

The cold noise power is calculated as:

$$N_C = k_B \cdot T_0 \cdot B = k_B \cdot 300 \text{ K} \cdot 2 \text{ MHz} \approx 8,28 \times 10^{-15} \text{ W} \approx -110,8 \text{ dBm} \quad (2.11)$$

The hot noise power is determined using the Excess Noise Ratio (ENR):

$$\text{ENR} = \frac{T_H - T_C}{T_0} \approx \frac{T_H}{T_C} \quad (2.12)$$

$$N_{H,\text{dB}} \approx N_{C,\text{dB}} + \text{ENR}_{\text{dB}} \approx -96,3 \text{ dBm} \quad (2.13)$$

### 2.3.3 Integration Time

Furthermore the sensitivity of the receiver eq. (2.2) depends on the integration Time  $\tau_I$ . Since noise, a statistical process, is measured, integration is required to determine a power average in the time window  $\tau_I$ . Generally speaking, higher integration times thus improve the sensitivity.

### 2.3.4 Gain Drift

In every receiver small drifts in gain  $\Delta G$  occur and because an increase in gain or increase in input power can not be distinguished, this worsens receiver sensitivity. In eq. (2.2) this is related to  $G_0$ , the average gain of the complete system, meaning that relative gain fluctuations are relevant to assess the sensitivity.

## 2.4 Bandwidth

A greater Bandwidth to measure noise, further increases sensitivity of the radiometer eq. (2.2). The RTL-SDR is specified with a maximum stable sample rate of 2.56MHz [4] and the HackRF is limited to an integer bandwidth setting, so a sample rate of 2 MHz was used for all SDR measurements to ensure consistency.

## 2.5 Radio Quiet Zone

To further lower noise coupled into the system, a frequency band to measure the sun should be chosen that is free from transmission of radio signals. According to the frequency plan of the federal network agency of Germany [3] the 10.6 - 10.68 GHz band was chosen. Using the low band of the LNB (LO Frequency of 9.7 GHz [13]), we want to measure an IF Frequency between 850MHz and 930 MHz. As the used noise source is specified at 1GHz with known ENR we decided to perform the measurements at an IF Frequency of 1GHz for all SDRs.

## 2.6 SDR internal signal chain

Essentially SDRs use an LNA at their input to amplify the incoming signal (This gain can later be defined by software). The LNA is crucial to ensure a low noise figure and low gain drift. Furthermore the gain ranges differ between the used SDRs, which limits the minimum input signal level. A mixer with a LO is used to mix the signal down and an Analog to Digital Converter with I/Q Sampling to retrieve amplitude and phase information. The latter comes with different resolutions for the different used SDRs, impacting their dynamic range as well as the maximum possible sample rate.

## 3 General Experimental Setups and Procedures

The experiments for this project were carried out on the 5th floor of the HFT building in the laser laboratory at TU Berlin. The equipment used is listed below, the experimental setups are described and the implementation is explained.

### 3.1 Laboratory equipment used

The signal generator *ROHDE & SCHWARZ SMPC* (fig. 12.1 left) is used, which is GPIB/SCPI controllable. To calibrate this, the spectrum analyzer *KEYSIGHT EXA Signal Analyzer N9010B* (fig. 12.1 right) is used, which is also GPIB/SCPI controllable. The used noise source is the *Agilent 346B* fig. 2.3. To power this the *KEYSIGHT E36234A Dual Output Autoranging DC Power Supply* (fig. 12.6) is used. Furthermore multiple coaxial cables are used.

### 3.2 Used SDRs

The SDRs that were tested are listed in table 3.1 with their respective TU Berlin RFID Codes.

Device	USRP B210	USRP B200 mini	ADALM Pluto	HackRF One	RTL-SDR
RF Range	70 MHz to 6 GHz	70 MHz to 6 GHz	325 MHz to 3.8/6 GHz	1 MHz to 6 GHz	500 kHz to 1.766 GHz
Bandwidth	56 MHz	56 MHz	20 MHz	20 MHz	2.4 MHz
ADC	12 bits	12 bits	12 bits	8 bits	8 bits
Price	3000€	1500€	250€	300€	35€
RFID Code	-	250102	240100	-	240030

**Table 3.1:** Comparison of SDR hardware specifications [8]

The USRP B200 mini is a more compact variant of the B200/B210 series from Ettus Research (NI) and shares many technical features with the B210, but with only one transmit and receive channel [14]. As can be clearly seen, the SDRs differ greatly in their key figures.

### 3.3 General Settings GNU Radio Signal Processing Chain

The signal generator from *ROHDE & SCHWARZ SMPC* and the SDRs are run at a center frequency of 1 GHz for all measurements (section 2.5). The sample rate of the SDRs is set to 2 MHz. The general signal processing of the SDRs in GNU Radio is as follows. At the beginning, the data runs through a DC blocker to filter out any DC offsets<sup>1</sup>. Then, the IQ signal is converted into power using

$$P = \text{Re}(x)^2 + \text{Im}(x)^2$$

The power is then logarithmized

$$P_{\text{dB}} = 10 \cdot \log_{10}(P)$$

Now the gain is subtracted<sup>2</sup>

$$P_{\text{dB, corrected}} = P_{\text{dB}} - G$$

The signal is then smoothed over 1000 samples using the moving average.

$$P_{\text{average}} = \frac{1}{1000} \sum_{i=1}^{1000} P_i$$

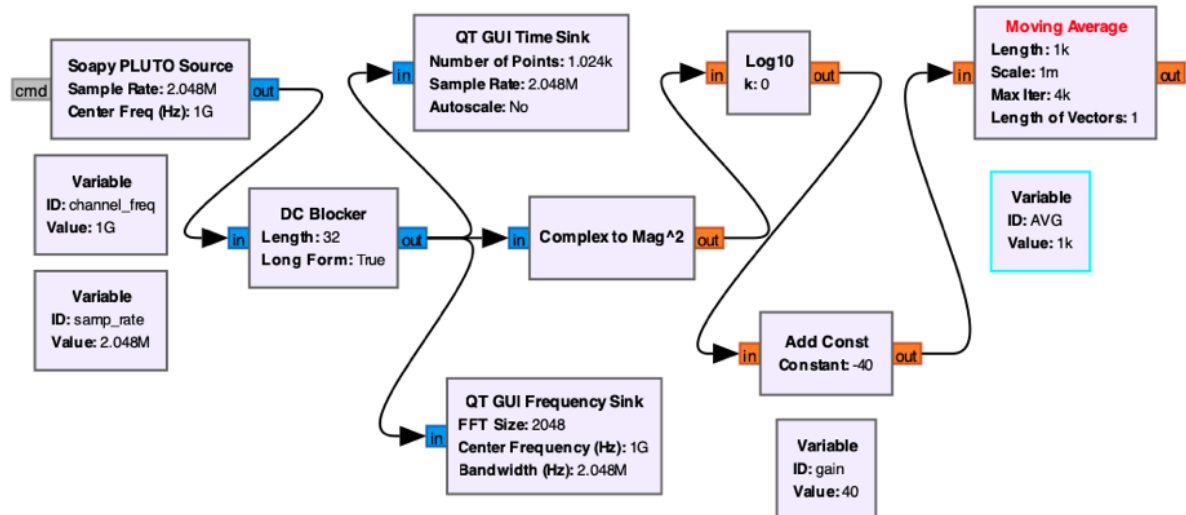


**Figure 3.1:** GNU Radio Signal Chain

<sup>1</sup>Note that in the experiments on dynamic range and gain drift, no DC blocker is used, since a continuous wave (CW) signal is placed at the center frequency and would otherwise be removed by the DC blocker.

<sup>2</sup>This subtraction is performed to infer the input power. However, it will be shown later that an additional offset distorts this estimation.



**Figure 3.2:** National Instruments GPIB to USB Adapter

## 3.4 Automation

Especially when measuring the dynamic range for multiple SDRs at various gain settings, the required measurement time is substantial. For each gain setting and SDR, 120 measurement points were recorded<sup>3</sup>, where the signal generator's output power is adjusted and the corresponding received power is logged. Automating this process not only significantly reduces the time required but also ensures repeatability, for example when testing different SDR models or firmware versions.

### 3.4.1 GPIB

A widely used interface with lab equipment is serial communication via GPIB. To connect a computer, a GPIB to USB Adapter by National Instruments (GPIB-USB-HS Adapter, fig. 3.2) is used.

---

<sup>3</sup>This corresponds to measurements taken over an input range from -120 dBm to 0 dBm with a step size of 1 dBm, as described later in the dynamic range experiment.

## GPIB Adapter communication

To interface with the specific Adapter, the backend NI-VISA is required to be installed [12]. The interface with the GPIB-USB-HS Adapter however only works successfully on windows.<sup>4</sup> Later, to embedd the control of the lab equipment into python programs, the library pyvisa is used that allows for simple control of the devices. First the GPIB Adress of the device needs to be requested. This can be done by running the `rm.list_resources()` command, where `rm` is previously initialized as in listing 3.1. Furthermore the commands for each device are different and can be looked up in the users and programers guide online<sup>5</sup>. The used Signal Generator comes with a sheet underneath with all commands as can be seen in fig. 12.12.

```

1 import pyvisa
2
3 rm = pyvisa.ResourceManager()
4 my_instrument = rm.open_resource('GPIBO::13::INSTR') # Connect to
   the device with GPIB Adress 'GPIBO::13::INSTR'
5
6 my_instrument.write(1000 MH -100 DB) #Send a command to the
   device, here: Set the output to 1GHz with -100dBm output level.

```

**Listing 3.1:** GPIB: Setup and send a command

For the signal generator listing 3.1 shows the relevant command for our applications, setting amplitude and frequency of the output. The spectrum analyzer, in contrast, requires significantly more configuration steps.

## Commands Keysight EXA

The following important commands were used for the Spectrum Analyzer to make appropriate measurement settings, where the values in curly braces are variables defined at the beginning of the program:

```

1 exa.write('*RST') # Reset
2 exa.write('*CLS') # Clear Status
3
4 exa.write(f'SENS:FREQ:CENT {CENTER_FREQUENCY_HZ} HZ') # Set
   Center Frequency
5 exa.write(f'SENS:FREQ:SPAN {SPAN_HZ} HZ') # Set Span
6 exa.write(f'SENS:BAND:RES {RESOLUTION_BW_HZ} HZ') # Set
   Resolution Bandwidth
7 exa.write('CALC:MARK1:MODE POS') # Set Marker with Peak Search
8 exa.write('SENS:AVER ON') # Activate Averaging

```

<sup>4</sup>For more detailed information see: <https://www.ni.com/de/support/documentation/compatibility/21/ni-hardware-and-operating-system-compatibility.html>

<sup>5</sup>The Keysight Spectrometers guide can be downloaded at [9]

```

9  exa.write(f'DISP:WIND:TRAC:Y:RLEV {REFERENCE_LEVEL_DBM} DBM') # 
    Set reference level
10 exa.write(f'SENS:POW:ATT {ATTENUATOR_DB} DB') # Set attenuator
    level
11 exa.write('SENS:POW:GAIN:STAT OFF') # Deactivate LNA
12 sweep_time_str = exa.query('SENS:SWE:TIME?') # query sweep time
13 exa.write('SENS:AVER:CLE') # Clear Averages
14 measured_power_str = exa.query('CALC:MARK1:Y?') # query measured
    power

```

**Listing 3.2:** used Commands Keysight EXA

### 3.4.2 Python embedding

As explained in detail in section 5.1, synchronization between the control of the laboratory equipment and the SDR is required. For this purpose, the flowgraphs created in GNU Radio are exported as Python files and extended with two threads, one for running the GNU Radio flowgraph and another for controlling the laboratory instruments. To execute the programs, the Radioconda environment [18] is installed and its shell is used to run the Python scripts, ensuring that all required libraries for GNU Radio operation are available.

On MacBooks using the Apple-Silicon Chips, the graphical GNU Radio interface does not work, however, the command-line interface version runs reliably, which is sufficient for this project. On Windows systems, additional drivers must be installed for each SDR to ensure proper functionality.

## 3.5 Repository

The complete set of scripts, automation tools, and guidelines for SDR characterization within the scope of this project is available at:

<https://github.com/daniel4828/SDR-Characterisation-for-Radio-Astronomy>

The repository is structured to allow independent use and can be used as a basis for characterizing SDRs beyond the scope of this project.

## 4 Calibration of the Signal Generator

The signal generator is central to the investigation of SDRs. In order to ensure that it outputs the expected power, it must be examined beforehand so that any offsets or similar deviations can be taken into account for the next tests.

### 4.1 Set Up

The signal generator *ROHDE & SCHWARZ SMPC* is examined. The spectrum analyzer *KEYSIGHT EXA Signal Analyzer N9010B* is used for this purpose. Both are connected with a coaxial cable. Furthermore, the clock of the signal generator is connected to that of the spectrum analyzer to synchronize both devices (fig. 12.3). Finally, both devices are connected to the laptop via USB-C (fig. 12.2) using a GPIB adapter to automate the measurement and read out the data. A sketch of the experiment can be seen in fig. 4.1 and the finished experimental setup in fig. 12.1.

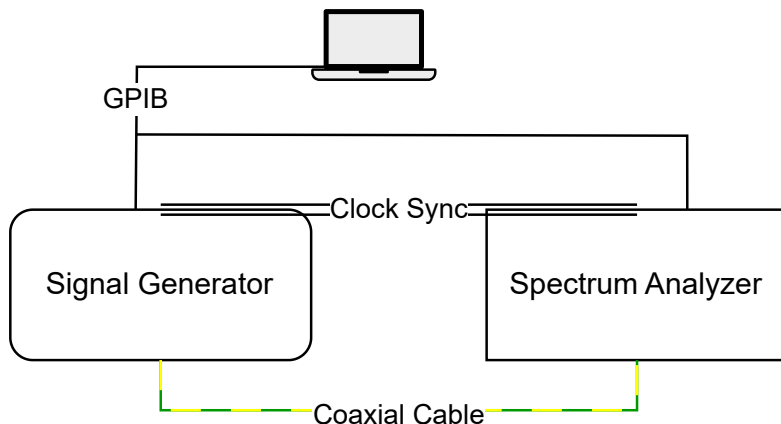


**Figure 4.1:** Setup Calibration Signal Generator

An automated measurement script in Python using the PyVISA library is used. This enables sequential control of both the signal generator and the spectrum analyzer *Keysight EXA N9010B* via the GPIB interface (see fig. 3.2).

The aim is to systematically vary the output power of the signal generator in the range of -120 dBm to 0 dBm, as this power range covers the measurement range relevant for the subsequent SDR characterization. The signal generator is operated at a frequency of 1 GHz. The center



**Figure 4.2:** Calibration Signal Generator finished Setup

frequency of the spectrum analyzer is therefore also set to 1 GHz with a span of 10 kHz. The spectrum analyzer records 100 samples for each data point and takes the average value.

The calibration is carried out in two separate measurement runs, with the range from -120 dBm to -95 dBm (*Low Range*) being examined in the first run and the range from -95 dBm to 0 dBm (*High Range*) in the second run. The division of the measurement is necessary because with the spectrum analyzers settings for the High Range, the noise floor is too high to measure the Low Range. In order to still obtain reliable measured values in the lower power range, the following settings in table 4.1 are selected for the measurements.

Setting	Low Range	High Range
Power Range	-120 dBm to -95 dBm	-95 dBm to 0 dBm
Resolution Bandwidth (RBW)	3 Hz	220 Hz
Reference Level	-40 dBm	0 dBm
Attenuator	10 dB	10 dB

**Table 4.1:** Settings for the calibration measurements in the low and high range

Thanks to the drastically reduced resolution bandwidth, the noise level can be significantly reduced so that even very low signal levels can be recorded. However, this improvement had a disadvantage. The reduced Resolution Bandwidth leads to significantly longer sweep times per data point, as the device required considerably more time for sufficient averaging (100 averages). A higher RBW is chosen for the high range (220 Hz) to keep the sweep time low and still receive good results at higher signal levels.

The output power of the signal generator is increased in 1 dB steps for the Low Range and High Range (table 4.1). After each change, the average value of the measured power is recorded over the previously defined number of averaging cycles. The measurement results are automatically written to a text file and stored.

## 4.2 Results

The measured power levels are shown as a function of the set input power in fig. 4.3. The figure includes two independent measurement series, recorded on different days, to assess reproducibility. A linear regression is applied to both data sets, as it provides a simple method for correcting systematic deviations in dynamic range through the calculation of slope and offset coefficients. Additionally, the ideal linear response is plotted for reference. The deviation between the measured data and the ideal curve is minimal, which confirms overall system linearity but makes it difficult to precisely evaluate small non-linear effects. The resulting regression coefficients are shown in eq. (4.1).

$$P_{measured} = 0,99 \cdot P_{set} - 1,22 \quad (4.1)$$

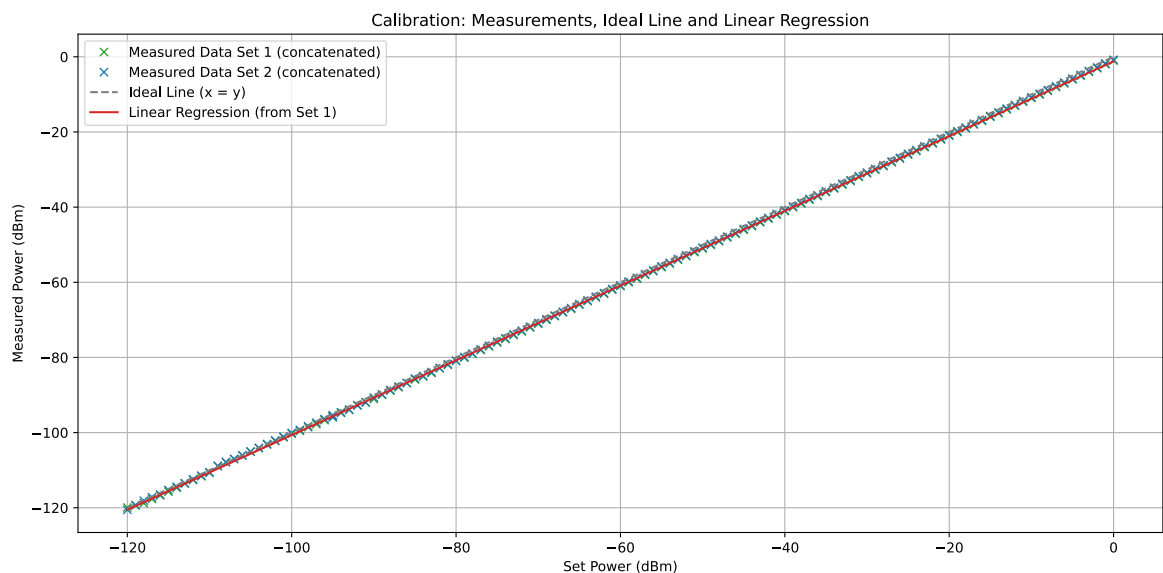


**Figure 4.3:** Set Power vs Measured Power and Regression and Ideal Line

A second plot, shown in fig. 4.4, illustrates two error metrics. First, the absolute error of the signal generator, defined as the difference between the set and the measured output power and second, the deviation between the measured values and the linear regression. The latter represents the remaining error after applying regression-based correction to the dynamic range measurements. The regression is based on the first calibration dataset, as the second dataset was acquired after the experimental phase had been completed. Its purpose is to estimate the calibration accuracy and stability over time.

As seen in fig. 4.4, the linear regression effectively compensates for the nearly constant offset observed for input levels above  $-80$  dBm. Below this threshold, the variance within one measurement series increases, and the two independent datasets no longer show a constant relative offset. This behavior is attributed to the reduced signal-to-noise ratio near the noise floor, which limits measurement precision at low input power levels.

Higher accuracy in this low-power range could be achieved by reducing the resolution bandwidth of the spectrum analyzer. However, this would substantially increase the measurement time. In the context of this project, a maximum deviation of less than 1 dBm from the regression is entirely acceptable.

Interestingly, no discontinuity is observed at the point where the resolution bandwidth changes ( $-95$  dBm), which might be expected. This suggests that the chosen spectrum analyzer settings (table 4.1) were appropriate and that the device's prior calibration conducted eight months earlier remains valid. The close agreement between the two independent measurement sets further confirms the stable and predictable behavior of the signal generator.

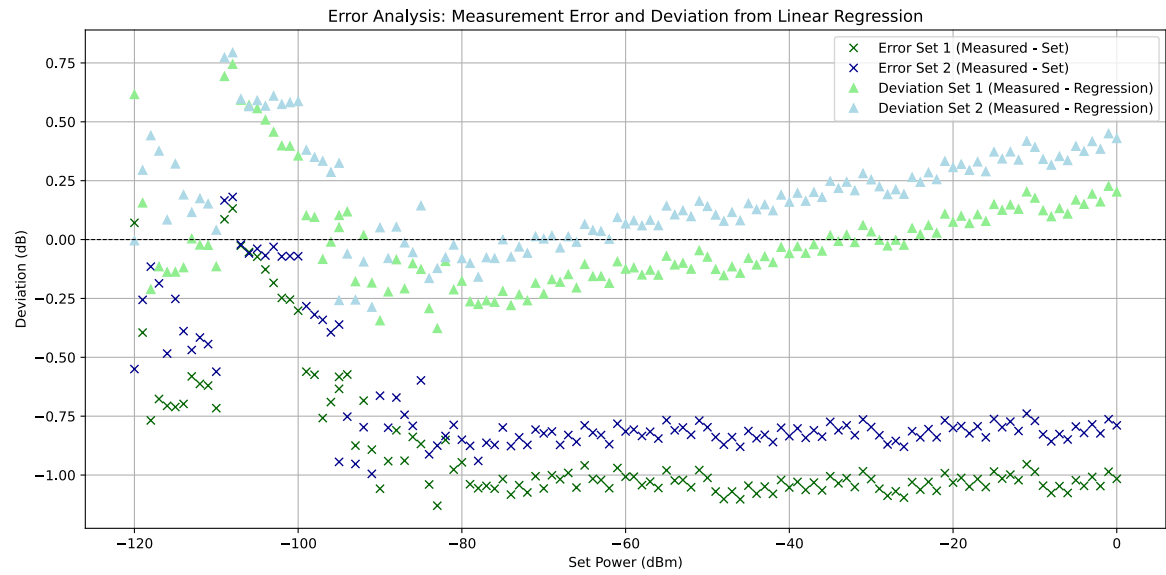


**Figure 4.4:** Comparison of error and deviation of the regression

## 5 Dynamic Range

The SDRs receive the input signal and returns it in the unit dBFS (Decibel relative to Full Scale). This unit describes the strength of a signal relative to the maximum displayable value of the ADC in the SDR. A value of 0 dBFS corresponds to the strongest possible signal. Negative dBFS values show how much weaker the signal is compared to the maximum display.

As dBFS is a relative value, there is no direct conversion to dBm. It must be determined individually beforehand what this mapping looks like.

The number of ADC bits used differs depending on the SDR. The Pluto SDR uses a 12-bit ADC, while the RTL-SDR only has 8 bits (table 3.1). If the signal is above or below this range, the signal is cut to the maximum or minimum value to be displayed with the bits. In order to be able to work with the SDRs, it is important to know how large this range is in each case.

### 5.1 Set Up

To determine this dynamic range, each SDR is connected via coaxial cable to the previously calibrated signal generator *ROHDE & SCHWARZ SMP*, as shown in fig. 5.2 and fig. 12.4. A SMA right angle adapter is used to avoid damaging the screw connection of the SDRs (fig. 12.5). It is important that the signal generator is now synchronized with its own or some other clock beforehand, otherwise no power will be output<sup>1</sup>. The SDR is then connected to the laptop via USB-C. The laptop is connected to the signal generator via the GPIB to USB-C adapter. The setup sketch can be found in fig. 5.1.

The measurement is carried out automatically with a Python script (section 3.5) which uses GNU Radio (section 3.3) and the pyvisa GPIB interface (section 3.4). At the beginning, the center frequency of the signal generator is set to 1 GHz. Then the output power is reduced on the signal generator in 1 dB steps from -120 dbm to 0 dbm. Each step takes 1 s. This signal now is measured with the SDR and its the basic GNU-Radio receiver chain (fig. 3.1). This process is performed for several possible gain settings. Each SDR, except for the RTL-SDR and the Hack RF, are measured in a gain range from 0 dB to 70 dB in 10 dB steps. The RTL-SDR only has a maximum gain of 49 dB and the Hack RF of 62 dB.

---

<sup>1</sup>Because the spectrum analyzer is no longer used, in contrast to the calibration experiment of the signal generator, where it provided a clock reference to the signal generator

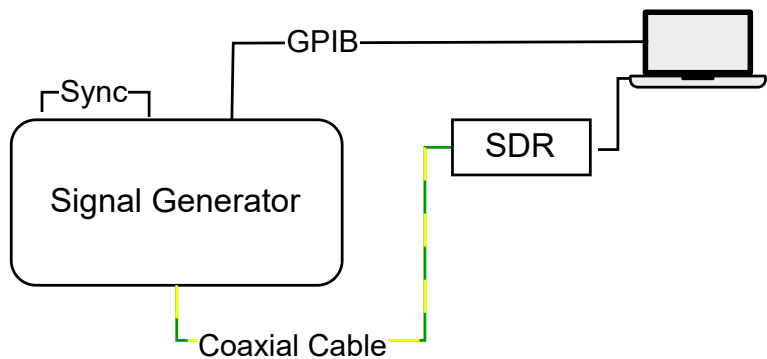


**Figure 5.1:** Sketched Setup Dynamic Range Experiment

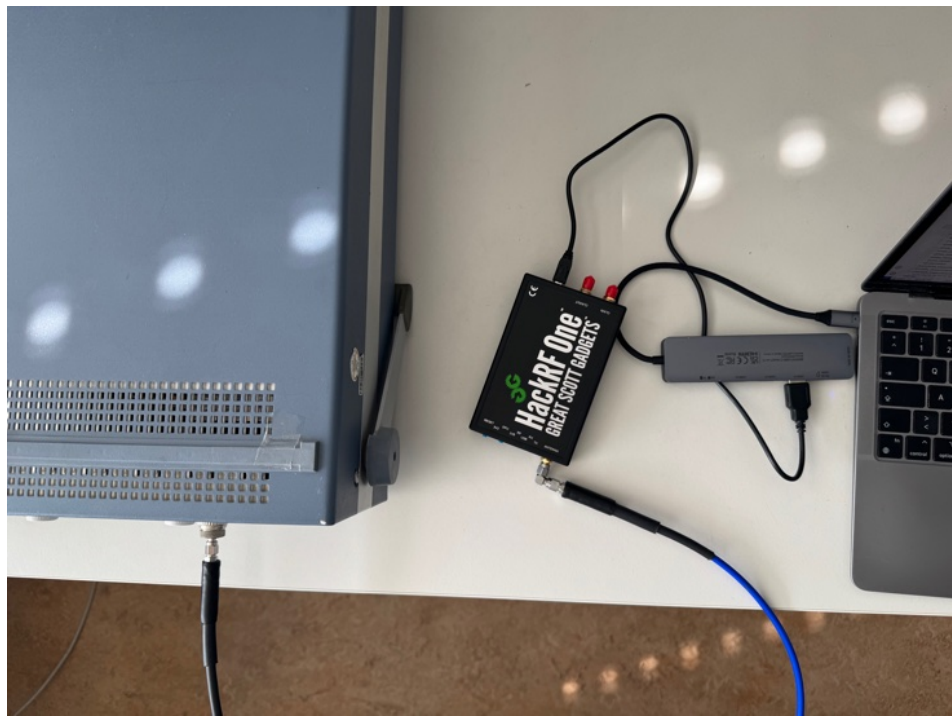


**Figure 5.2:** Finished Setup for examining the Dynamic Range of a SDR with a signal generator

## 5.2 Estimation of SDR Input Power

In order to utilize the measurement values specifically for use in a radiometer, it is necessary to determine a reference value for an expected input level of the SDR when using it for measuring the sun's temperature. Since, at the time of writing this report, no measurement has yet been carried out, due to bad weather conditions. So the input level was estimated to be around -59 dBm. How this estimate was arrived at can be found in section 12.2.

Knowing this expected output power is essential to assess whether the selected SDR is sufficiently sensitive to detect such signal levels. It serves as a benchmark for verifying that the input power lies within the linear and detectable range of the SDR, ensuring reliable operation in the intended radiometric application.

## 5.3 Results

fig. 5.3 shows the dynamic range measurement results for the Pluto SDR. It shows the available input power vs. the measured output power. As expected, higher gain settings result in higher output power. To make the results across different gain values comparable, the respective gain is subtracted as an offset from each measurement, as illustrated in fig. 5.4.

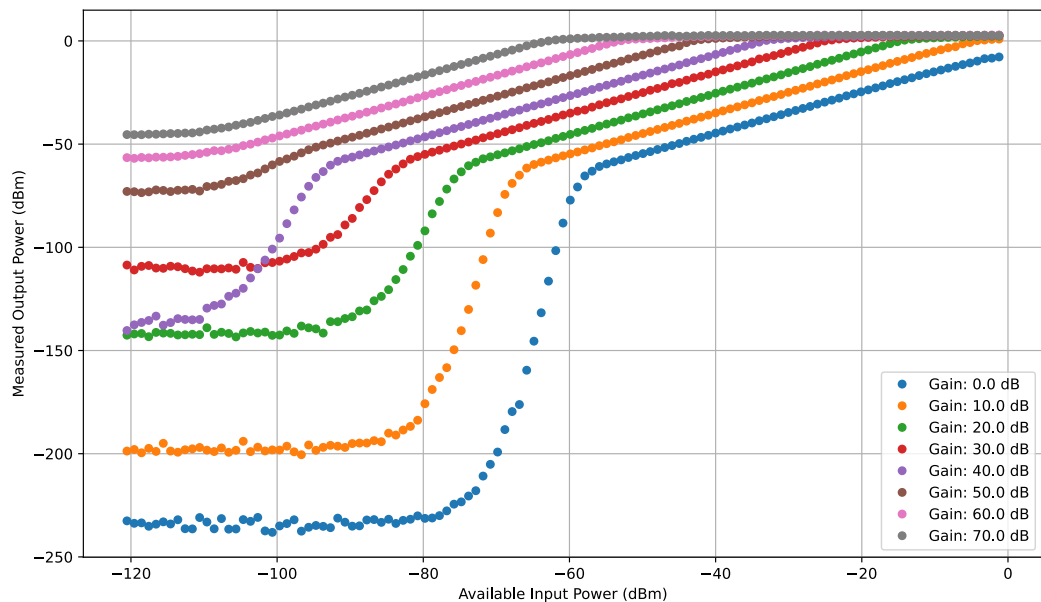


**Figure 5.3:** Dynamic range of the Pluto SDR: measured output power vs. available input power for various gain settings.

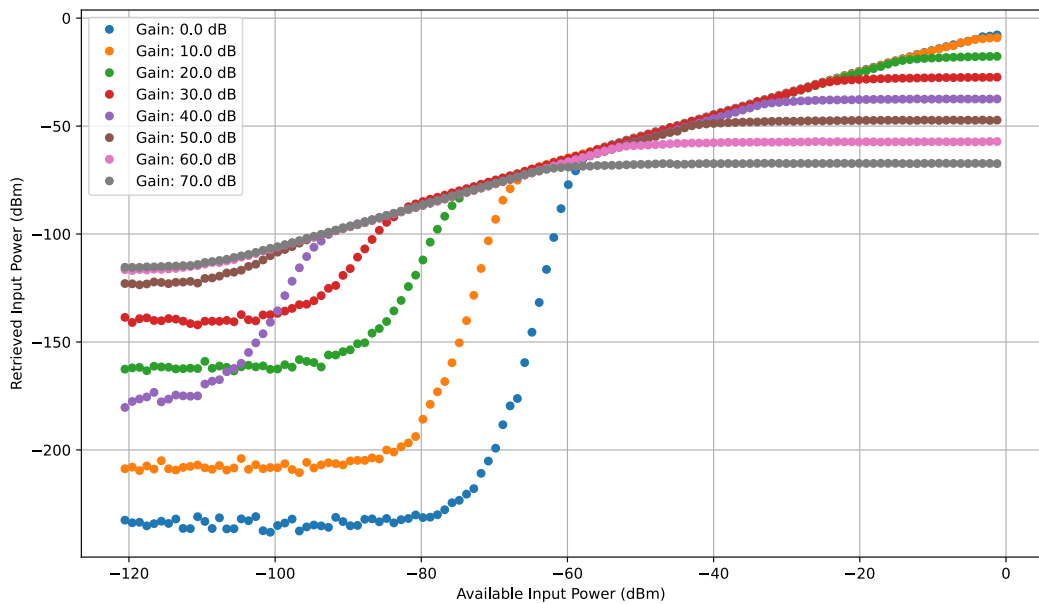


**Figure 5.4:** Dynamic range of the Pluto SDR after gain correction: retrieved input power vs. available input power for various gain settings.

As seen in fig. 5.3, the measured output power does not exceed 0 dBm. Strictly speaking, the measured output power in fig. 5.3 (or the retrieved input power in fig. 5.4) must be corrected by the offset listed in table 5.1, in order to convert the measurement — which is initially only interpretable as a dBFS value — into an equivalent dBm value. This apparent limitation reflects the 0 dBFS ceiling of the ADC: once the input power is high enough to drive the converter into saturation, all ADC bits are set to one, and thus the reported value cannot exceed this threshold. For low input power levels, the output power drops off sharply. In this region, the Pluto SDR can no longer be operated reliably, as the signal becomes too weak to be accurately represented by the available ADC bits.

Each gain setting is evaluated using linear regression to find the longest interval in which the relationship between input and output power remains highly linear. The results are summarized in table 5.1 for the PLUTO SDR and in section 12.3.2 for all other SDRs which is the main outcome of the dynamic range analysis. The tables show the input power range for each gain setting where the SDR operates linearly. The *Offset-Gain* value must be subtracted from the calculated signal-chain power (see fig. 3.1) to convert a measurement initially expressed in dBFS into a meaningful dBm value. The *Offset* value is the same as the *Offset – Gain* value but with the gain added and should be used if the gain is not subtracted in the signal chain, unlike in fig. 3.1. If every gain stage amplified perfectly, the value of *Offset – Gain* would remain constant across all settings and the Offset Value would rise accordingly with an increase of the Gain.

Additionally, the dynamic range and ENOB (according to eq. (2.3)) were calculated to indicate the size of the linear input window for each gain setting. The ENOB indicates the number of

bits an ideal analog-to-digital converter (ADC) would need to achieve the same dynamic range as the actual ADC. The ENOB is generally lower than the nominal ADC resolution of each SDR (see table 3.1), with the HACK RF (table 12.1) showing particularly poor utilization of its ADC bits. Surprisingly, the USRP SDRs (table 12.3, table 12.4) exhibit an ENOB exceeding their actual ADC resolution at certain gain settings, which contradicts theory and remains unexplained. The reduction in ENOB is caused by nonlinearities near the edges of the linear range and by the strict linearity criterion imposed.

### 5.3.1 Pluto SDR

For the Pluto SDR, the *Offset – Gain* value varies. Between 0 dB and 30 dB gain, the variation is small at only 0.532 dB. For higher gain values, the variation increases. This means that a fixed offset value cannot be applied across all gain settings. Instead, a separate offset must be determined for each gain in order to achieve accurate results.

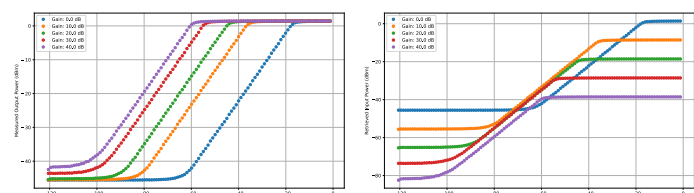
If the gain settings are adjusted accordingly, the Pluto SDR can detect input powers in the range from  $-2,213 \text{ dBm}$  to  $-108,613 \text{ dBm}$ . This corresponds to a wide and well-usable dynamic range for radiometric measurements and includes the in section 5.2 calculated value of  $-59 \text{ dBm}$ .

Gain	Input Power Range [dBm]	Offset	Offset - Gain	DR [dB]	ENOB
0.0	$[-57,899; -2,213]$	-4,850	-4,850	55,686	8,87
10.0	$[-66,848; -2,213]$	4,883	-5,117	64,635	10,39
20.0	$[-74,803; -11,162]$	14,618	-5,382	63,641	10,28
30.0	$[-83,753; -22,101]$	25,136	-4,864	61,652	10,00
40.0	$[-93,697; -29,061]$	32,984	-7,016	64,636	10,39
50.0	$[-100,658; -39,960]$	43,323	-6,677	60,698	9,82
60.0	$[-111,596; -50,938]$	51,365	-8,635	60,658	9,81
70.0	$[-108,613; -60,882]$	60,572	-9,428	47,731	7,67

**Table 5.1:** Identified linear input power ranges and offset values for each gain setting of the Pluto SDR. These ranges define the effective dynamic range where the device operates linearly.

### 5.3.2 RTL-SDR

The output power measurements of the RTL-SDR are shown in fig. 12.17, the retrieved input power in fig. 12.18, and the linear input power ranges per gain setting are summarized in table 12.2, which also shows the number of ADC bits needed. A noticeable feature in



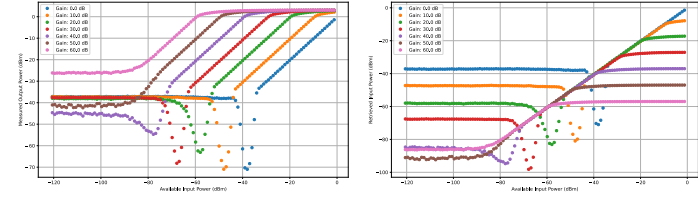
Left: measured output power; Right: retrieved output power. See full plots in Appendix figs. 12.17 and 12.18.

fig. 12.17 is the varying spacing between the curves. This is also reflected in the values of table 12.2. For the RTL-SDR, the offset must therefore be determined individually for each gain setting.

Compared to the Pluto SDR, fig. 12.17 also clearly shows the lower cutoff caused by the ADC at low input power levels. Although the RTL-SDR only supports gain settings up to 49,6 dB, it still achieves a usable dynamic range from  $-101,652$  dBm to  $-16,134$  dBm. This range is smaller than that of the Pluto SDR but still larger than the dynamic range of the HackRF.

### 5.3.3 HackRF SDR

The maximum configurable gain of the HackRF is 62 dB. Regarding the ADC-related cutoffs, the HackRF behaves like a combination of the Pluto SDR and the RTL-SDR. At low input power levels, the measured output power initially drops sharply after leaving the linear range but then stabilizes again around  $-10$  dBm. For gain settings up to 40 dB, a clear cutoff becomes visible, as shown in fig. 12.15 and fig. 12.16. The reason for this behavior is unclear.



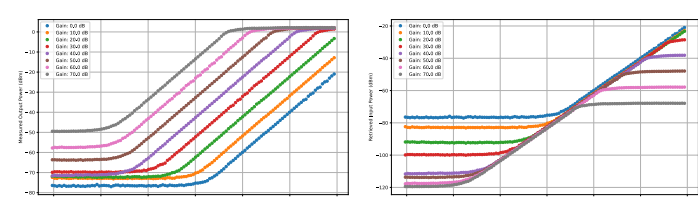
Left: measured output power; Right: retrieved output power. See full plots in Appendix figs. 12.15 and 12.16.

The offsets between gain settings fluctuate more than with the Pluto SDR, but considerably less than with the RTL-SDR, as seen in table 12.1. The overall usable dynamic range of the HackRF extends from  $-1,219$  dBm to  $-82,759$  dBm, which makes it the SDR with the smallest usable dynamic range among all devices tested.

Especially when compared to the RTL-SDR, this is a disadvantage for our use case, as both devices rely on 8-bit ADCs. One possible explanation is the wide RF range of the HackRF. As shown in table 3.1, it covers the broadest frequency span among the tested SDRs.

### 5.3.4 USRP B210

The USRP B210, which is the most expensive SDR in this comparison, offers a usable dynamic range from  $-95,686$  dBm to  $-1,219$  dBm, as shown in table 12.3. Despite its price, this range is smaller than that of the significantly more affordable Pluto SDR.



Left: measured output power; Right: retrieved output power. See full plots in Appendix figs. 12.21 and 12.22.

After applying gain correction (Offset – Gain), the resulting Offset –

Gain values remain within a relatively narrow band between  $-20,15$  dB and  $-24,61$  dB. This indicates a fairly consistent systematic deviation across the entire gain range.

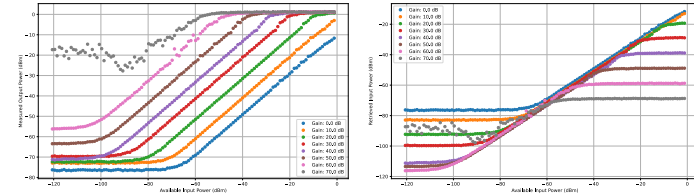
Regarding the linear input power intervals, it can be observed that for low gain values ( $0$ – $20$  dB), the usable range increases primarily at the lower end toward weaker input signals, while the upper limit remains nearly constant at around  $-1,2$  dBm. Starting from a gain of  $30$  dB, the upper limit also begins to shift downward. Beyond  $40$  dB of gain, however, any further expansion of the dynamic range is minimal. The lower limit continues to decrease only slowly, while the upper limit remains nearly unchanged. This suggests that the amplifier stage reaches its limit and the usable range begins to saturate.

On average, the linear range measurable at each gain setting is significantly larger than for the other SDRs, with the exception of the USRP B200 Mini.

In fig. 12.21 and fig. 12.22, linear regions are clearly identifiable. However, slight irregularities appear at gain levels of  $0$  dB,  $30$  dB, and  $60$  dB. The cause of these anomalies is unknown, but a similar pattern is observed with the USRP B200 Mini. This could indicate a general issue in the architecture of the USRP series.

### 5.3.5 USRP B200 Mini

The fluctuations already observed with the USRP B210 are significantly more pronounced in the USRP B200 Mini, as shown in fig. 12.19 and fig. 12.20. At a gain of  $60$  dB, these variations become clearly noticeable and increase further at  $70$  dB, to the point where this gain setting can no longer be used reliably, even though it is officially supported according to [14].



Left: measured output power; Right: retrieved output power. See full plots in Appendix figs. 12.19 and 12.20.

The overall usable dynamic range spans from  $-1,219$  dBm to  $-99,663$  dBm. However, beyond a gain of  $40$  dB, there is almost no further improvement in measurable performance. The data therefore suggest using  $40$  dB as a practical upper limit, since measurement instability increases at higher gain values. Using higher gains than  $40$  dB can however be practical to achieve a lower noise figure as examined in chapter 8.

As with the USRP B210, the linear range that can be measured per gain setting is larger than that of the other SDRs.

All tested SDRs show significant differences in their dynamic range behavior and require individual characterization. The gain values provided by the manufacturers do not correspond

directly to the actual amplification in terms of absolute power output. Therefore, each gain setting must be individually measured and evaluated to determine the effective operating range.

Importantly, all SDRs are able to reliably detect an input power level of  $-59 \text{ dBm}$ , as estimated in section 5.2, confirming their general suitability for use in the radiometer system.

The Pluto SDR shows the most consistent and stable behavior across all gain settings. It delivers a wide overall dynamic range with minimal variation and no significant anomalies, making it the most reliable and predictable device among those tested.

## 6 Gain Drift

The accuracy of long-term radio astronomical measurements relies on a stable gain. A temporal drift in gain will distort the results, as it cannot be distinguished from a genuine change in signal power at the input, which directly reduces measurement accuracy.

### 6.1 Setup

This measurement is performed using a splitter (fig. 12.10) to allow parallel testing of all SDRs. While the use of the splitter reduces the input power from the signal generator by approximately 20 dB at each output, the absolute input power level is not critical in this context. Only the relative variation of the measured power over time is evaluated.

The actual measurement setup is shown in fig. 6.2, and a schematic overview of the configuration is provided in fig. 6.1.

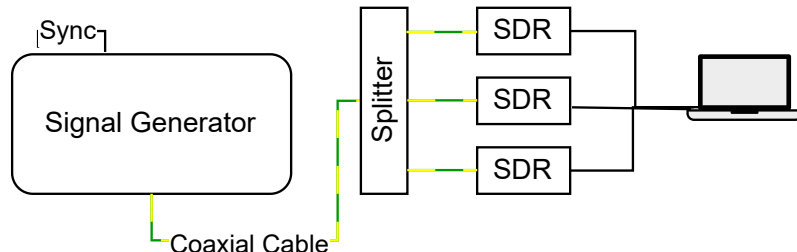


**Figure 6.1:** Gain Drift Measurement Setup Sketch



**Figure 6.2:** Gain Drift Setup with Splitter

To investigate the gain drift, the *Rohde & Schwarz SMPC* signal generator is used again. It is connected to the splitter via a coaxial cable (fig. 12.10) at the splitters RX IN port. The RX outputs are then connected to the SDRs using coaxial cables (fig. 12.11). One output remains unused and is also terminated with a  $50\Omega$  load (The connections of the splitter can be seen in more detail in fig. 12.11). All six DRX ports and the DRX IN port of the splitter are terminated with  $50\Omega$  loads. The SDRs are connected to a laptop, which is in general capable of interfacing with multiple SDRs simultaneously.

With the splitter all SDRs receive the same input power. Nevertheless the different SDRs gains do not perform the same, so one SDR might amplify the input signal so much that is out of the SDRs the dynamic range, whereas another does not. To ensure all SDRs operate within their linear dynamic range, three input power levels were determined. The goal was to maintain a consistent gain setting across all devices. However, due to the different dynamic ranges of the SDRs, the gain for the RTL-SDR and HackRF sometimes had to be adjusted to keep the input signals in their optimal, linear operating region. The gain settings and input power levels shown in table 6.1 were selected.

Set Input Power [dBm]	Est. Real Input Power [dBm]	RTL-SDR	PlutoSDR	USRP mini B200	USRP B210	HackRF
-10	-30	0 dB	0 dB	0 dB	0 dB	10 dB
-37	-57	20 dB	30 dB	30 dB	30 dB	40 dB
-55	-75	40 dB	60 dB	60 dB	60 dB	60 dB

**Table 6.1:** Gain settings of each SDR for different input power levels. The estimated real input power accounts for approximately 20 dB attenuation due to the splitter.

In principle, the measurement can be conducted over any desired duration. However, due to limited laboratory time, only one measurement was performed over 30 minutes: the one with an input power of  $-57$  dBm, because it closely corresponds to the estimated input power calculated in section 5.2. The measurements at the other two input levels were conducted over a duration of only 15 minutes to save time.

In total two separate measurement series (different days) were performed, each with the above described setup, to detect possible inconsistencies.

## 6.2 Results

To better visualize the general trend, the measurement results are smoothed.

For the RTL SDR, a 15-minute and a 30-minute measurement of the first measurement series are shown in 6.5. It is noticeable that for the 40dB Gain setting, despite the shorter measurement duration, the gain drift is significantly stronger than for the 20dB gain setting. Given the reasons mentioned, we decided to perform the second measurement series as stated above in the setup description. This is also the reason why some of the plotted trends, or all of them, as in fig. 6.5, are only 15 minutes long: Only the worst-case scenarios are considered to compare the SDRs to one another.

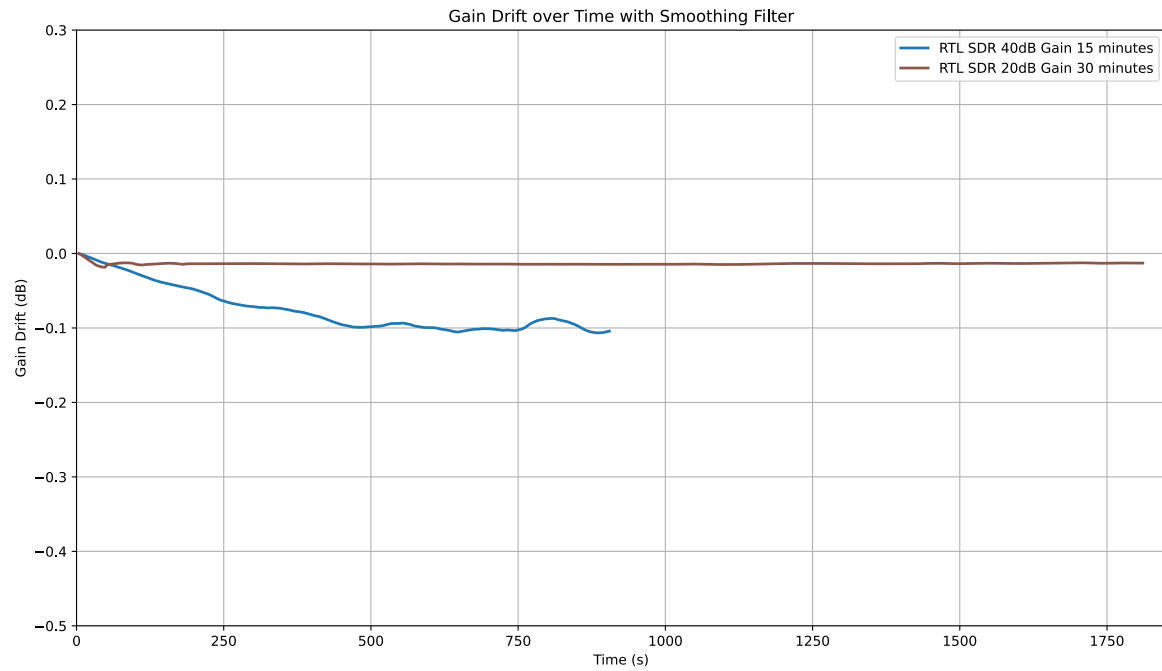


**Figure 6.3:** Comparison of 15 minute and 30 minute gain drift result for RTL SDR in measurement series 1

In fig. 6.4 and fig. 6.5, the worst-case scenarios of two independent gain drift measurement series conducted on different days are shown. Both indicate that the Pluto SDR and the USRP B210 consistently exhibit the smallest gain drifts. Furthermore, in both measurement series, it can be observed that the HackRF shows a poor gain drift of greater than 0.4 dB. The RTL SDR and the USRP B200 unfortunately show different behaviors in the two measurement series. Nevertheless, it is noteworthy that the magnitude of the gain drifts in both measurement series is very comparable, with a maximum deviation of slightly above 0.4 dB over 15 minutes (RTL SDR). It is also noteworthy that in the second measurement series fig. 6.5, all worst cases occurred at the same input power for the 15 minutes measurement <sup>1</sup>.

<sup>1</sup>However, a correlation with a gain drift of the signal during this specific measurement can be excluded, since the traces of the Pluto SDR and USRP B210 do not show any significant gain drift.

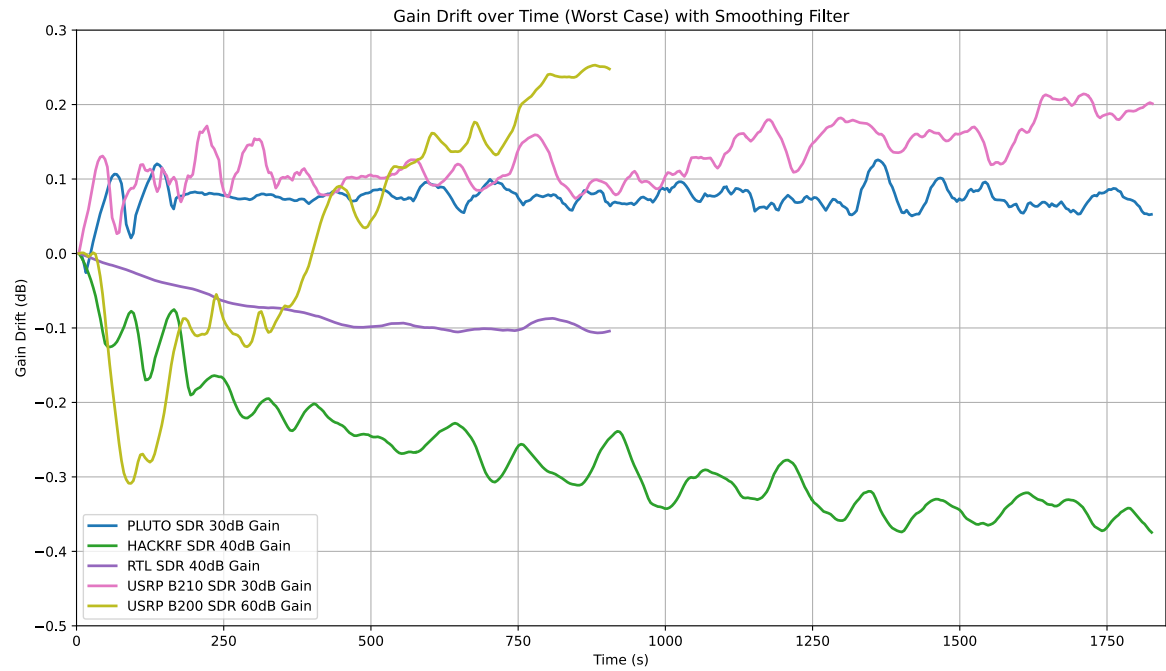


**Figure 6.4:** Gain Drift Worst Cases Measurement series 1 (showing only the gains with the strongest gain drift)

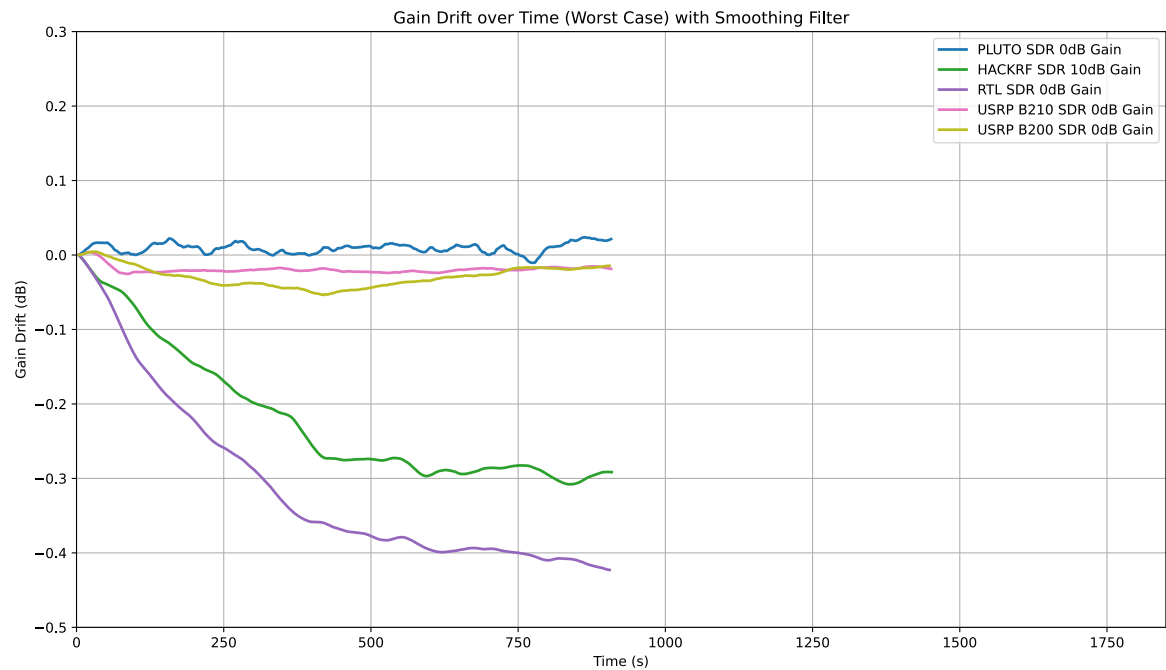


**Figure 6.5:** Gain Drift Worst Cases Measurement series 2 (showing only the gains with the strongest gain drift)

### 6.3 Drift at expected Radiometric Input Power

To evaluate the measurement results in relation to the complete project goal of measuring the sun's temperature, a third plot fig. 6.6 was created, in which only the worst cases of both 30-minute measurement series are presented, since the input power applied to the SDR for these measurements (Table 6.1) at -57 dBm is very close to the reference value of the expected input power when measuring the sun (section 5.2).

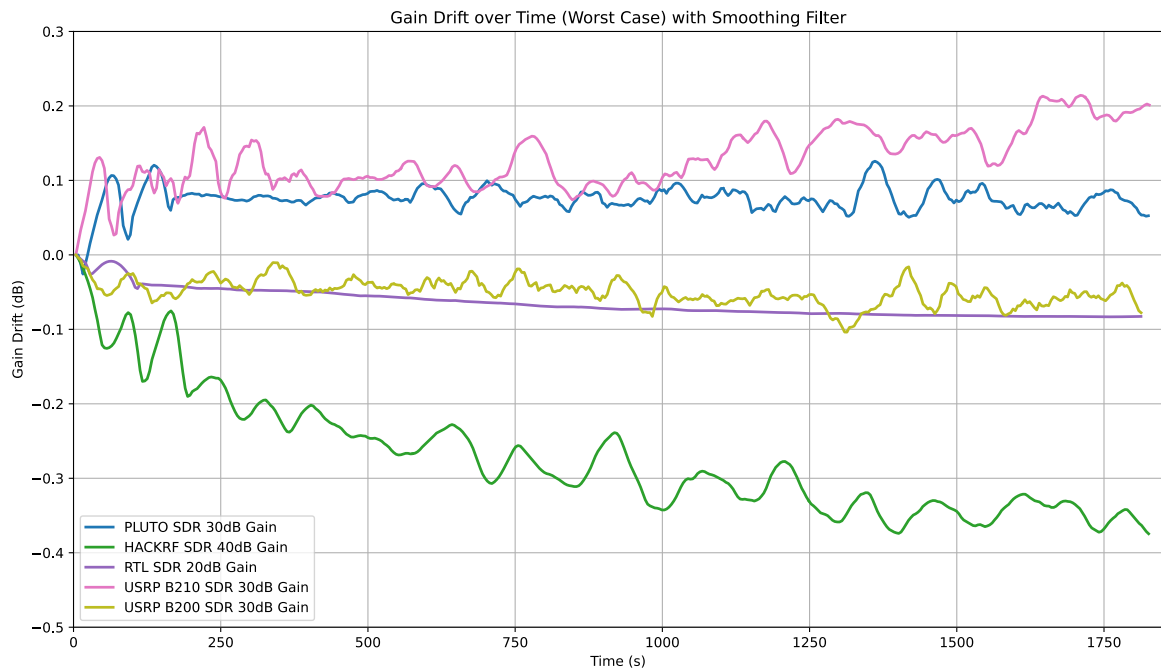


**Figure 6.6:** Gain Drift Worst Cases for both 30 Minute Measurement series

### 6.4 Temperature Dependence

An important factor influencing gain drift is temperature. In [2], it was investigated and confirmed that the gain can be well described by a linear relationship with temperature. However, this relationship cannot be confidently correlated with our measurement results, since the ambient temperature (constant at 27°C in both measurement series) is not decisive, but rather the temperature of the SDRs themselves. It was, however, observed that the RTL SDR (large gain drift in measurement series 2) became significantly heated after a period of use, whereas the USRP B210 (small gain drift in all measurement series) could dissipate heat much more effectively due to its large metallic enclosure and did not exhibit any noticeable heating even after prolonged operation. It is therefore worth examining to what extent gain drift can be related to temperature.

## 6.5 Estimation of Receiver Sensitivity

In order to evaluate the magnitude of the gain drift in the context of this project, an estimation of the achievable temperature measurement accuracy is carried out in section 12.4.1 using eq. (2.2).

For this purpose, the worst case among all measurements is selected, with a gain drift of -0.43 dB (RTL SDR in fig. 6.5) which gives an accuracy of 46K. Additionally, a second calculation is performed using the worst case of the best SDR in the measurement series, with a +0.13 dB gain drift (Pluto SDR within the 30-minute window in fig. 6.4) which gives an accuracy of 15K.

It becomes clear that the choice of SDR has a significant impact on measurement accuracy. It should also be noted that in eq. (12.4), a 30-minute instead of a 15-minute interval was used, which means that despite the improved accuracy, a longer calibration interval could be chosen.

## 6.6 Improvement of Investigation

Nevertheless, these estimations should be treated with caution and primarily illustrate an evaluation approach. To calculate reliable values, a known gain drift of the LNB is required. Additionally, the gain drift experiment should be repeated multiple times, since the deviating results for the RTL SDR and USRP strongly suggest that different experimental conditions can significantly affect the results. It is particularly advisable to continue investigating the Pluto SDR to find an appropriate gain setting where the input level during solar observation lies within the dynamic range and where the gain can then be adjusted to minimize gain drift, as this SDR showed the smallest gain drifts in both measurement series. A more detailed investigation would also benefit from recording the exact temperatures of the SDRs and LNBs, in order to achieve gain drift compensation based on the findings in [2].

## 7 Integration Time

The sample rate used is 2 M Samples/s. To handle this large amount of data, multiple data points are combined into a single measurement value by integrating over a specific time interval. With increasing integration time  $\tau$ , more data points are included in the averaging process. Since noise signals are naturally subject to statistical fluctuations, the question arises as to the optimal integration time  $\tau$  that minimizes these fluctuations and thus ensures the best possible measurement accuracy.

### 7.1 Set Up

For this measurement, the setup is sketched in (fig. 7.1 and shown with real parts in fig. 7.2). An *Agilent 346B* serves as the noise source, which is powered by a *Keysight EX36243A* DC source. The noise source generates a statistical noise signal with a known ENR of 14.54 dB. The output of the noise source is connected to the SDR via an external LNA [11], which was modified with a usb cable to easily connect power.

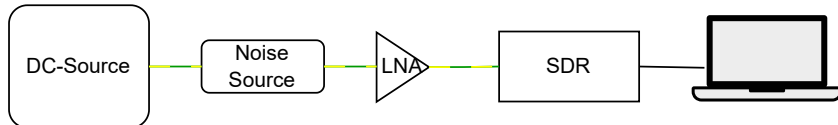


**Figure 7.1:** Integration Measurement Sketch



**Figure 7.2:** Finished Setup to determine Integration Time

The noise source is operated continuously at 28 V. The signal output by the noise source is amplified by the LNA and then fed to the SDR. Internally, the signal processing takes place as shown in fig. 3.1. Data is collected over a period of 120 s. This measurement is repeated for different gain settings.

### 7.1.1 Initial Approach and Lessons Learned

In the first attempt, only a  $50\Omega$  termination was connected to the SDR input, as a noise input and the Allan deviation was calculated for different time intervals across various gain settings. The fundamental problem with this approach was that its thermal noise (according to eq. (2.11)) does not fall within the dynamic range of the SDRs. When operating outside the dynamic range, the Noise Floor dominates the result which is not meaningful for the use in the application.

The new approach uses the turned on calibrated noise source fig. 2.3 with an additional external LNA so that the signal level is well within the dynamic range of most tested SDRs. The used LNA was measured with a spectrometer to have a gain of 15,24 dB which means that gains with a minimum input power of -81,06 dBm or lower can be specified (value from eq. (2.13) amplified by LNA gain)<sup>1</sup>. This highlights the critical importance of proper signal level management in SDR-based measurements.

---

<sup>1</sup>For which gain settings this condition is fulfilled can be checked with the tables conducted in the dynamic range experiment section 12.3.2.

## 7.2 Results

The Allan deviation is a statistical measure for quantifying the temporal stability of a signal. In contrast to the classical standard deviation, which does not converge for many noise-affected signals, the Allan deviation provides a robust method for evaluating the variation of mean values over adjacent time intervals  $\tau$ . Originally developed for analyzing frequency stability in oscillators, it proves to be extremely helpful in signal analysis of noisy signals with low amplitude.

For the analysis, the Allan deviation of the recorded signal is calculated. This indicates how much the mean value changes over adjacent time intervals  $\tau$  and thus serves as a measure of the temporal stability of the signal. The integration time intervals  $\tau$  are distributed logarithmically between 0.1 s and 100 s. Through this method, it is possible to determine which integration time enables optimal noise smoothing without losing useful information [19].

The results for the USRP B210 are presented in fig. 7.3 as a log-log plot. The measurements exhibit the characteristic behavior predicted by [15]. The Allan deviation initially decreases with increasing integration time, reaching a minimum before rising again. For example, at a gain setting of 60 dB, the minimum Allan deviation occurs at approximately 10 s.

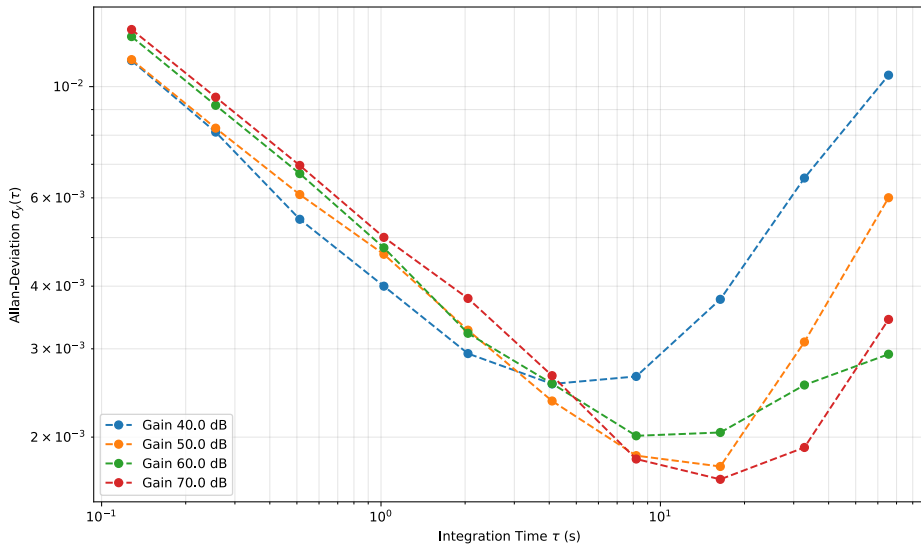


**Figure 7.3:** Allan deviation for different integration time intervals for several gains of the USRP B210, first measurement set

This characteristic trend of initial decrease followed by an increase can be explained by the competing effects of statistical averaging and systematic drifts. In the initial phase, longer integration times improve the signal-to-noise ratio through statistical averaging of the white noise component, resulting in lower Allan deviations. This occurs because increasing the averaging time reduces the uncertainty by including more independent samples in the measurement.

However, beyond the optimal integration time, systematic effects begin to dominate. Long-term drifts in the SDR's gain, temperature variations, and other slow-varying instabilities introduce

correlated noise that cannot be reduced by simple averaging. These systematic effects cause the characteristic upturn observed in the measurements. The optimal integration time represents the crossover point where white noise reduction is balanced by the onset of systematic drift effects.

The measurement results for the Pluto SDR are presented in fig. 7.4 and for the USRP B200 mini in fig. 12.24. Here the lowest gain setting behave different, showing first a drop, then a rise and finally again a drop of the allan deviation for longer integration times. This does not align with the trend for all other gain settings. This anomalous behavior of the measurement values at the lowest gain settings for both the Pluto SDR and the USRP B200 mini indicates that the actual noise level was lower than theoretically calculated of -81 dB. Consequently, these gain settings were outside the suitable measurement range for this investigation. Paradoxically, this initially false-appearing measurement confirms the problematic nature of the original approach using the  $50\Omega$  termination.

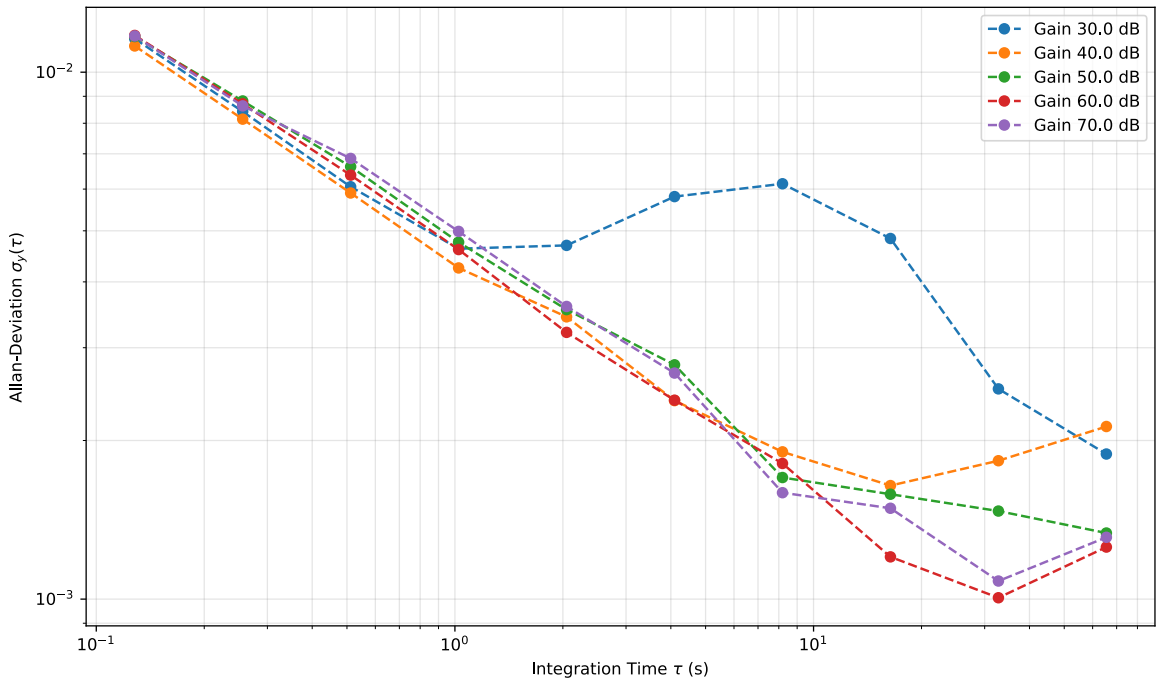


**Figure 7.4:** Allan Deviation for different integration time intervals for several gains of the Pluto SDR, first measurement set

The optimal integration time values  $\tau$  for the USRP B200 mini lie in similar ranges to those of its larger counterpart, the B210 (see fig. 7.3). For the Pluto SDR, the Allan deviation was calculated for gain values starting from 30 dB, with the results shown in fig. 7.4. This measurement series should be repeated with considerably more time, as the characteristic rise in Allan deviation is only barely discernible. The optimal integration time points therefore presumably lie at higher values than for the USRP series.

For the HackRF, the measurement could only be performed at a gain setting of 60 dB due to its limited dynamic range. This measurement clearly exhibits the expected behavior, as shown in fig. 12.23, with an optimal integration time of 1 s. This value is significantly shorter than those observed for the other SDRs.

The measurements for the RTL-SDR are shown in fig. 12.28 and behave as expected.

The trend predicted by [15] of decreasing and subsequently increasing Allan deviation with increasing integration time could be reproduced. The corrected experimental methodology lends significantly more credibility to these results compared to previous measurements, where the SDRs were operated completely outside their intended dynamic range.

However, several important questions remain unanswered and warrant further investigation. The relationship between higher gain settings and optimal integration time is not yet fully understood. Additionally, the significant variation in optimal integration times between different SDR platforms ranging from 1 s for the HackRF to approximately 10 s for the USRP series indicates that the underlying factors determining these values are SDR-dependent and require further clarification.

In a second measurement series, the results could be confirmed (see Figures 12.25, 12.26, 12.27, 12.28, 12.29). Figures 12.30 and 12.31 exemplify measurement results from this original HackRF measurement method ( $50\Omega$  termination), showing that the measurement results were not reproducible. For this reason, the remaining presented measurements in this thesis are taken solely from the second measurement setup.

## 8 Noise Figure

For precise radiometric measurements, it is essential to know the noise figure (NF) of the receiver chain. The NF indicates how much additional noise is introduced by the receiving system itself and is therefore critical for the correct interpretation of the measured signal power.

To determine the NF of the SDRs, the so-called *Y-factor method* is used (section 2.3.2).

### 8.1 Set Up

An *Agilent 346B* noise source is used, powered by a *Keysight EX36243A* DC supply at 28 V. The noise source generates a statistical noise signal with a known excess noise ratio (ENR) of 14.54 dB. Its output is connected to the SDR via a low-noise amplifier (LNA [11]). The complete setup is shown schematically in fig. 8.1 and as a photograph in fig. 12.8.

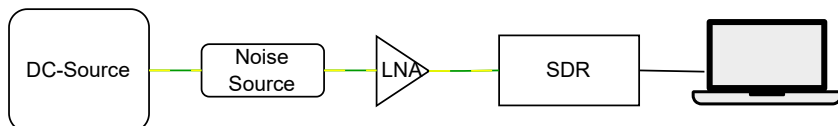


**Figure 8.1:** Noise Figure Measurement Sketch

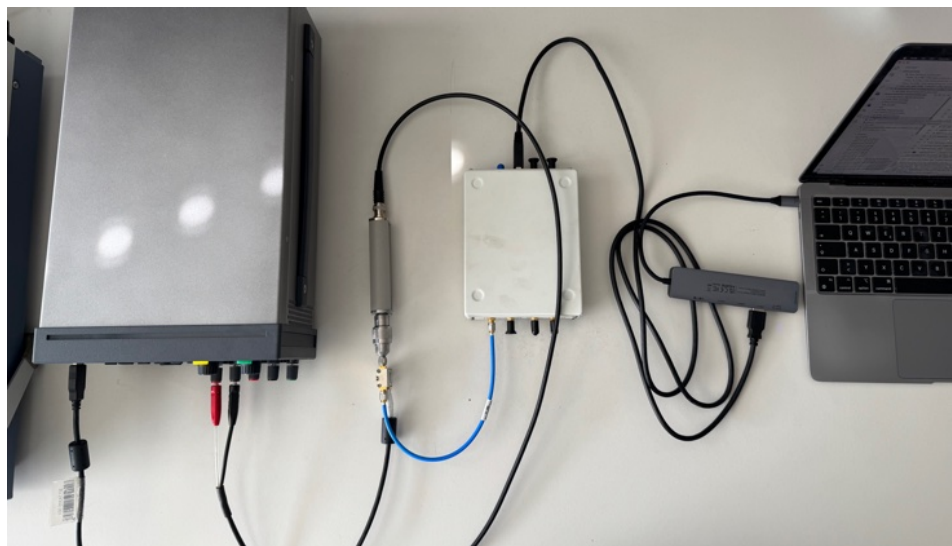


**Figure 8.2:** Finished Setup to determine Noise Figure

The noise source is first switched on (hot state). After a short settling time, the received power is measured over a duration of 4 seconds. The noise source is then switched off (cold state), and the power is measured again for another 4 seconds. The Y-factor is calculated from the ratio of the measured powers in the hot and cold states, as described in section 2.3.2.

## 8.2 Results

As calculated in 2.11 the noise power output of the calibrated noise source when turned off (thermal noise) equals -110.8 dBm. This constrains drastically the measureable gain settings for the SDRs, as described in 2.3.2. The used LNA was measured with a spectrometer to have a gain of 15,24 dB which means that smaller gains with a linear behaviour from -95,56 dBm of input power and on can be specified with a Noise Figure.

Unfortunately this means that the HACKRF and the USRP B200 mini are not at all able to give results with this method. To extend the measurable gain range, it may be beneficial to increase the bandwidth of the SDR where possible as this directly increases the received noise power (see eq. (2.1)). However, this effect is only significant if the bandwidth can be increased substantially, due to the logarithmic scale used in dBm.

All non-relevant measurement points are identified based on the results of the dynamic range analysis. Since the SDRs are intended to operate at high gain settings in the radiometric application, these limitations are acceptable within the context of the use case.

The fig. 8.3 shows that for all SDRs, the noise figure decreases as the gain increases. This behavior is typical for a cascaded system (fig. 2.2), where the second stage dominates the overall noise figure. In this context, the first stage refers to the internal LNA at the RF input, while the second stage includes the BALUN, Mixer, and A/D converter of the SDR.

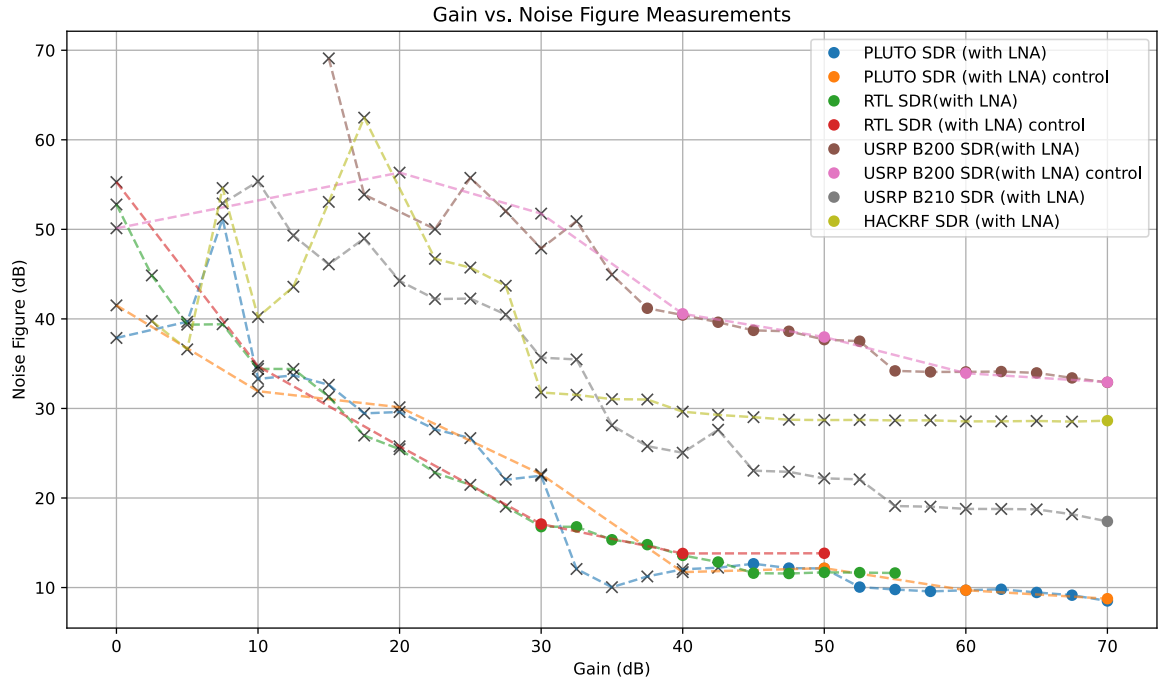


**Figure 8.3:** Noise Figure Measurements with LNA correction for different gain settings with marking of non-relevant points

According to eq. (2.7), increasing the gain of the first stage leads to a linear reduction of the total noise figure (on a dB scale), which matches the observed measurement trend.

The LNA causes the measured noise figure to appear lower than the actual noise figure of the SDR. To correct for this, the entire receiver chain must be considered, taking into account both the gain and noise figure of the LNA. According to eq. (2.7), the actual noise figure of the SDR can be calculated using the following relation:

$$F_{\text{SDR}} = (F_{\text{measured}} - F_{\text{LNA}}) \cdot G_{\text{LNA}} + 1 \quad (8.1)$$

Surprisingly, the USRP B200, despite being the second most expensive SDR in the comparison, performs the worst in terms of noise figure, reaching a minimum value of 33 dB. This is particularly unexpected given that its datasheet [5] specifies a maximum noise figure of 8 dB. One possible explanation is that the front-end may be optimized for higher frequencies, as the device supports an RF range of up to 6 GHz [5].

The Pluto SDR achieves the lowest noise figure among all tested devices when operated at high gain. Remarkably, the RTL-SDR performs equally well under high-gain conditions, which is noteworthy given the significant difference in price between the two devices.

To verify the measurement results particularly those of the USRP B200, which appeared unexpectedly high a second test series was performed. In this run, gain was increased in 10 dB

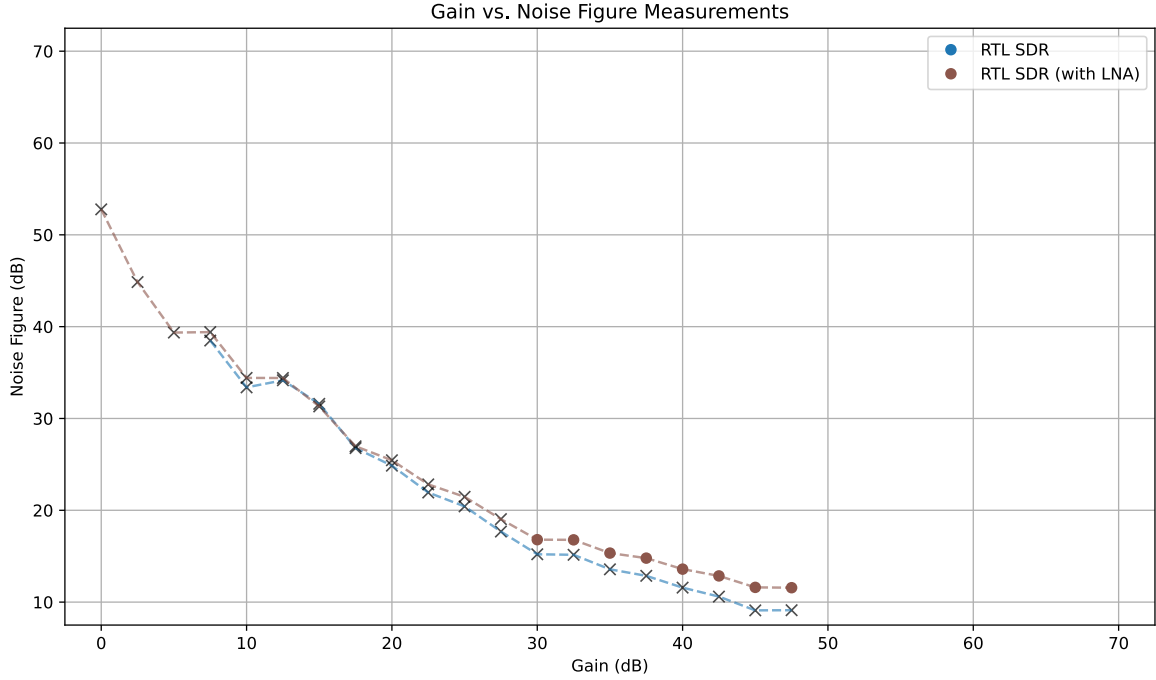


**Figure 8.4:** Comparison of Noise Figure Measurement with and without LNA

steps to reduce measurement time. As shown in fig. 8.3, the results closely matched those of the initial measurement, confirming the observed behavior.

To further validate that the use of the LNA does not distort the results, an additional measurement was conducted without the LNA in the chain, using the RTL-SDR (fig. 8.4). However, the RTL-SDR is not ideally suited for this test, since the cold noise power without LNA lies below the dynamic range for all available gain settings. As a result, the measured cold noise power is overestimated, which leads to a reduced Y-factor and thus an increased calculated noise figure (see eq. (2.8) and eq. (2.9)). Interestingly, fig. 8.4 shows that this expected behavior is not fully observed. The measured noise figure with LNA is actually higher than without it. This suggests that the correction using the full system chain (as described in eq. (2.7)) may be inaccurate, possibly due to an incorrect value for the LNA's noise figure. The noise figure used in the correction was taken from the datasheet [11], while the LNA gain was independently measured using a spectrum analyzer and found to be 15.24 dB instead of the specified 15.6 dB.

Nevertheless, the results with and without LNA (fig. 4.4) are generally in good agreement, which supports the overall validity of the measurement setup. Furthermore, any uncertainty in the LNA's noise figure would affect all measurements equally, preserving the relative comparability of the results across all SDRs. A comparison of the measurement results for the RTL-SDR was also made with those reported in [p.156, 16] for the gain range of 30–50 dB. The values fall within a similar range. However, in our setup, higher noise figures are observed at low gain settings and lower noise figures at high gain settings compared to the referenced study. This discrepancy could be caused by a nonlinearity in the LNA used in our measurement setup.

### 8.2.1 Noise Figure in complete Receiver Chain

The significance of the SDRs' noise figure must also be evaluated in the context of the complete receiver chain shown in fig. 2.1 with the LNB. Since the gain and noise figure of the LNB have not been measured directly, values from [13] are used instead. For a worst-case analysis, the lowest documented LNB gain is assumed ( $G_{\text{LNB}} = 50 \text{ dB}$ ). A representative worst-case noise figure of 20 dB is assumed for the SDR. In practical use cases involving high gain, such as with the RTL-SDR or Pluto SDR, the actual noise figure is significantly lower, as shown in fig. 8.4.

The overall system noise figure is calculated using the Friis formula as given in eq. (2.7). eq. (8.2) shows that, due to the high LNB gain, the contribution of the SDR's noise figure to the total system noise figure becomes negligible.

$$F_{\text{total}} = 10^{\frac{0,5}{10}} + \frac{10^{\frac{20}{10}} - 1}{10^{\frac{50}{10}}} \approx 1,12 + 9,9 \cdot 10^{-4} \quad (8.2)$$

For future measurements, it is strongly recommended to precisely characterize the noise figure of the LNA within the relevant power range. This ensures that correction calculations for the complete receiver chain yield accurate results. Additionally, the linearity of the LNA at low-level noise inputs should be investigated, as nonlinear behavior could distort the measured results.

## 9 Conclusion

The Pluto SDR is to be evaluated as the most suitable. It showed the smallest and most stable gain drift, which is important for precise long-term measurements. In contrast, the HackRF showed a high gain drift of over 0.4 dB, which makes it less suitable for this application. The RTL-SDR and the USRP B200 mini showed inconsistent behavior in various measurement series, indicating potential reliability issues. The USRP B210, similar to the Pluto SDR, consistently showed a low gain drift. Thus, the low gain drift of the Pluto SDR enables a calculated temperature resolution of about 15K, while the worst measured drift of the RTL-SDR limits the resolution to around 46K, assuming the unrealistic case of a non-existent LNB gain drift.

The analysis of the noise figure showed that although measurable differences exist between the SDRs, due to the high gain of the LNB in the receiver chain, the SDR's noise figure has a negligible impact on the overall system noise figure. Therefore, this metric is not heavily weighted in the final evaluation.

### 9.1 Usage Recommendation

When using the SDRs for scientific measurements operating in the correct dynamic range is crucial: For meaningful results, the SDR must be operated within its linear dynamic range. The characterization led to tables (e.g., 5.1) that should be used to select an appropriate gain setting.

To minimize measurement noise without being affected by system drifts, it is important to choose the correct integration time. These times varied depending on the device, with the HackRF having a short optimal integration time of 1 second and the USRP series around 10 seconds. The Pluto SDR showed a trend towards even longer optimal integration times, indicating higher stability.

### 9.2 Future Investigations

To complete a comprehensive result of the characterization of the receiver chain, we believe it is particularly important to conduct the following investigations: First, with the parabolic dish and LNB, the output level range of the LNB should be determined when observing the sun under different weather conditions, in order to specifically align further measurement series with this.

It is recommended to investigate the PlutoSDR more closely. The gain drift measurement should be repeated multiple times and also with an input level corresponding to the expected output

level range of the LNB, for even more representative statements. Of particular importance, however, is to characterize the gain drift of the LNB in order to put it in relation to that of the SDR.

If its gain drift exceeds the orders of magnitude of the SDRs, then the use of the RTL SDR should be considered instead for cost savings.

Furthermore, for this case, we recommend investigating compensation using the method in [2] by attaching precise temperature sensors, especially to the LNB.

To provide a more accurate classification of the radiometer's precision, it is also important to verify the noise figure of the LNB specified in [13].

## 10 List of Figures

2.1	Receiver Chain . . . . .	8
2.2	Cascaded system with Gain and Noise Figure per stage [10] . . . . .	10
2.3	calibrated noise source . . . . .	10
2.4	Y-Facor method hot and cold source measurement [1] . . . . .	11
3.1	GNU Radio Signal Chain . . . . .	14
3.2	National Instruments GPIB to USB Adapter . . . . .	15
4.1	Setup Calibration Signal Generator . . . . .	18
4.2	Calibration Signal Generator finished Setup . . . . .	19
4.3	Set Power vs Measured Power and Regression and Ideal Line . . . . .	20
4.4	Comparison of error and deviation of the regression . . . . .	21
5.1	Sketched Setup Dynamic Range Experiment . . . . .	23
5.2	Finished Setup for examining the Dynamic Range of a SDR with a signal generator	23
5.3	Dynamic range of the Pluto SDR: measured output power vs. available input power for various gain settings. . . . .	24
5.4	Dynamic range of the Pluto SDR after gain correction: retrieved input power vs. available input power for various gain settings. . . . .	25
6.1	Gain Drift Measurement Setup Sketch . . . . .	30
6.2	Gain Drift Setup with Splitter . . . . .	30
6.3	Comparison of 15 minute and 30 minute gain drift result for RTL SDR in measurement series 1 . . . . .	32
6.4	Gain Drift Worst Cases Measurement series 1 (showing only the gains with the strongest gain drift) . . . . .	33
6.5	Gain Drift Worst Cases Measurement series 2 (showing only the gains with the strongest gain drift) . . . . .	33
6.6	Gain Drift Worst Cases for both 30 Minute Measurement series . . . . .	34
7.1	Integration Measurement Sketch . . . . .	36
7.2	Finished Setup to determine Integration Time . . . . .	37
7.3	Allan deviation for different integration time intervals for several gains of the USRP B210, first measurement set . . . . .	38
7.4	Allan Deviation for different integration time intervals for several gains of the Pluto SDR, first measurement set . . . . .	39
8.1	Noise Figure Measurement Sketch . . . . .	41
8.2	Finished Setup to determine Noise Figure . . . . .	41

8.3	Noise Figure Measurements with LNA correction for different gain settings with marking of non-relevant points . . . . .	43
8.4	Comparison of Noise Figure Measurement with and without LNA . . . . .	44
12.1	Calibration Signal Generator finished Setup . . . . .	53
12.2	GPIB Connection to Signal Generator . . . . .	54
12.3	Clock Synchronisation of Signal Generator . . . . .	55
12.4	Dynamic Range Experiment Front Setup . . . . .	55
12.5	SMA Right Angle Adapter . . . . .	56
12.6	Keysight EX36243A DC Source . . . . .	57
12.7	Pluto SDR connected to Noise Source . . . . .	57
12.8	Finished Setup to determine Noise Figure . . . . .	58
12.9	Noise Figure Measurement Sketch . . . . .	58
12.10	Splitter . . . . .	58
12.11	Splitter with Coaxial cable . . . . .	58
12.12	Manual and GPIB Commands for Signal Generator . . . . .	59
12.13	Results for the Dynamic Range of the Pluto SDR. Measured output power vs available input power for different gain settings. . . . .	61
12.14	Results for the Dynamic Range of the Pluto SDR but it is shown the retrieved input power vs the available input power for different gain settings, meaning the gain was subtracted from the measured output power. . . . .	62
12.15	Results for the Dynamic Range of the HackRF SDR. Measured output power vs available input power. . . . .	63
12.16	Results for the Dynamic Range of the HackRF SDR but it is shown the retrieved input power vs the available input power for different gain settings, meaning the gain was subtracted from the measured output power. . . . .	64
12.17	Results for the Dynamic Range of the RTL-SDR. Measured output power vs available input power. . . . .	65
12.18	Results for the Dynamic Range of the RTL-SDR but it is shown the retrieved input power vs the available input power for different gain settings, meaning the gain was subtracted from the measured output power. . . . .	66
12.19	Results for the Dynamic Range of the USRP B200mini. Measured output power vs available input power. . . . .	67
12.20	Results for the Dynamic Range of the USRP B200mini but it is shown the retrieved input power vs the available input power for different gain settings, meaning the gain was subtracted from the measured output power. . . . .	68
12.21	Results for the Dynamic Range of the USRP B210. Measured output power vs available input power. . . . .	69
12.22	Results for the Dynamic Range of the USRP B210 but it is shown the retrieved input power vs the available input power for different gain settings, meaning the gain was subtracted from the measured output power. . . . .	70
12.23	Allan Deviation for different integration time intervals for several gains of the HackRF SDR, first measurement set . . . . .	73
12.24	Allan Deviation for different integration time intervals for several gains of the USRP B200 mini, first measurement set . . . . .	73

12.25Allan Deviation for different integration time intervals for several gains of the Pluto SDR, second measurement set . . . . .	74
12.26Allan Deviation for different integration time intervals for several gains of the USRP B210, second measurement set . . . . .	74
12.27Allan Deviation for different integration time intervals for several gains of the USRP B200 mini, second measurement set . . . . .	75
12.28Allan Deviation for different integration time intervals for several gains of the RTL SDR, second measurement set . . . . .	75
12.29Allan Deviation for different integration time intervals for several gains of the Hack RF, second measurement set . . . . .	76
12.30Allan Deviation for different integration time intervals for several gains of the HACKRF, wrong measurement setup, first measurement set . . . . .	76
12.31Allan Deviation for different integration time intervals for several gains of the HACKRF, wrong measurement setup, second measurement set . . . . .	77

## 11 Bibliography

- [1] Federico Alimenti. *Measuring the Microwave Noise*. guest lecture at TU Berlin. Feb. 2025.
- [2] Stefano Bonafoni et al. "An Efficient Gain Estimation in the Calibration of Noise-Adding Total Power Radiometers for Solar Observation: From Education to Science". In: *IEEE Transactions on Geoscience and Remote Sensing* 56.9 (2018), pp. 5289–5296. ISSN: 0196-2892. DOI: 10.1109/TGRS.2018.2807904.
- [3] Bundesnetzagentur für Elektrizität, Gas, Telekommunikation, Post und Eisenbahnen. *Frequenznutzungsplan*. last update: 14. Januar 2021. Bundesnetzagentur. URL: [https://data.bundesnetzagentur.de/Bundesnetzagentur/SharedDocs/Downloads/DE/Sachgebiete/Telekommunikation/Unternehmen\\_Institutionen/Frequenzen/20210114\\_frequenzplan.pdf](https://data.bundesnetzagentur.de/Bundesnetzagentur/SharedDocs/Downloads/DE/Sachgebiete/Telekommunikation/Unternehmen_Institutionen/Frequenzen/20210114_frequenzplan.pdf) (visited on 07/28/2025).
- [4] S. Carl and Contributors. *About RTL-SDR*. Specifications of the RTL-SDR. rtl-sdr.com. 2025. URL: <https://www rtl-sdr com/about-rtl-sdr/> (visited on 07/28/2025).
- [5] Ettus Research. *USRP B200/B210 Series: High-Performance, Bus-Powered SDR/Cognitive Radio*. Product Specification Sheet. National Instruments. Jan. 2019. URL: [https://www.ettus.com/wp-content/uploads/2019/01/b200-b210\\_spec\\_sheet.pdf](https://www.ettus.com/wp-content/uploads/2019/01/b200-b210_spec_sheet.pdf) (visited on 07/30/2025).
- [6] Robin Getz. *ADALM-PLUTO Detailed Specifications*. <https://wiki.analog.com/university/tools/pluto/devs/specs>. Specifications of the Pluto SDR. Feb. 2021. (Visited on 08/22/2025).
- [7] Great Scott Gadgets. *HackRF One Documentation*. [https://hackrf.readthedocs.io/en/latest/hackrf\\_one.html](https://hackrf.readthedocs.io/en/latest/hackrf_one.html). Specifications of the HackRF SDR. 2021. (Visited on 08/24/2025).
- [8] Dennis Jurk et al. *Radio Astronomy Project 2024 – Work Package 200: Receiver Design & Temperature Compensation*. Tech. rep. RA-24-WP200. Version 1.0. Department of Aeronautics and Astronautics, Office F 6. Berlin, Germany: Technische Universität Berlin, Chair of Space Technology, Aug. 2024.
- [9] Keysight Technologies. *Keysight 82357B USB/GPIB Interface User's Guide*. Part Number: 9018-06099. Keysight Technologies. July 2014. URL: <https://www.keysight.com/us/en/assets/9018-06099/user-manuals/9018-06099.pdf> (visited on 07/28/2025).
- [10] Leyo. "Darstellung einer Kettenschaltung von drei Verstärkern Berechnung der Gesamttrauschzahl mit Hilfe der Friis-Formel". Figure in: Wikipedia-article "Friis formulas for noise". Jahr des letzten Zugriffs. URL: <https://commons.wikimedia.org/wiki/File:Friis-Kette.svg>.

- [11] Mini-Circuits. *ZX60-P103LN+: Ultra-Low Noise Amplifier, 10 MHz to 3000 MHz*. Data Sheet for ZX60-P103LN+. Mini-Circuits. Mar. 2017. URL: <https://www.minicircuits.com/pdfs/ZX60-P103LN+.pdf> (visited on 07/30/2025).
- [12] National Instruments. *NI-VISA Download*. Download-Page for the NI-VISA-backend. National Instruments. 2025. URL: <https://www.ni.com/de/support/downloads/drivers/download.ni-visa.html#570633> (visited on 07/28/2025).
- [13] SP3SWL Paweł. *Testing the Othernet "Bullseye BE01" LNB*. Information about the LO-frequency, the gain and the noise figure of the Bullseye LNB. pabr.org. 2025. URL: <https://www.pabr.org/radio/otherlnb/otherlnb.en.html#> (visited on 07/28/2025).
- [14] Ettus Research. *USRP B200/B210/B200mini/B205mini Series – Technical Overview*. Accessed: 2025-07-27. 2025. URL: <https://kb.ettus.com/B200/B210/B200mini/B205mini>.
- [15] Giacomo Schiavolini et al. “Low-Cost Calibrated Microwave Radiometers for Solar Observation: From Education to Science”. In: *Proceedings of the IEEE Radio and Wireless Symposium (RWS)*. San Antonio, TX, USA, 2024.
- [16] Giacomo Schiavolini et al. “Low-Cost Calibrated Microwave Radiometers for Solar Observation: From Education to Science”. In: *Proceedings of SIE 2024*. Ed. by Maurizio Valle, Paolo Gastaldo, and Ernesto Limiti. Vol. 1263. Lecture Notes in Electrical Engineering. Springer Nature Switzerland, 2025, pp. 142–159. ISBN: 978-3-031-71518-1. DOI: 10.1007/978-3-031-71518-1\_17.
- [17] M. E. Tiuri. “Radio Astronomy Receivers”. In: *IEEE Transactions on Military Electronics* 8.3 (1964), pp. 264–272. DOI: 10.1109/TME.1964.4323154.
- [18] Ryan Volz. *Radioconda*. Repository with installationmanual and information about SDR-drivers. GitHub. 2025. URL: <https://github.com/ryanvolz/radioconda> (visited on 07/29/2025).
- [19] Wikipedia contributors. *Allan variance — Wikipedia, The Free Encyclopedia*. Accessed: 2025-07-29. 2025. URL: [https://en.wikipedia.org/wiki/Allan\\_variance](https://en.wikipedia.org/wiki/Allan_variance).

## 12 Appendix

### 12.1 Setup Photos

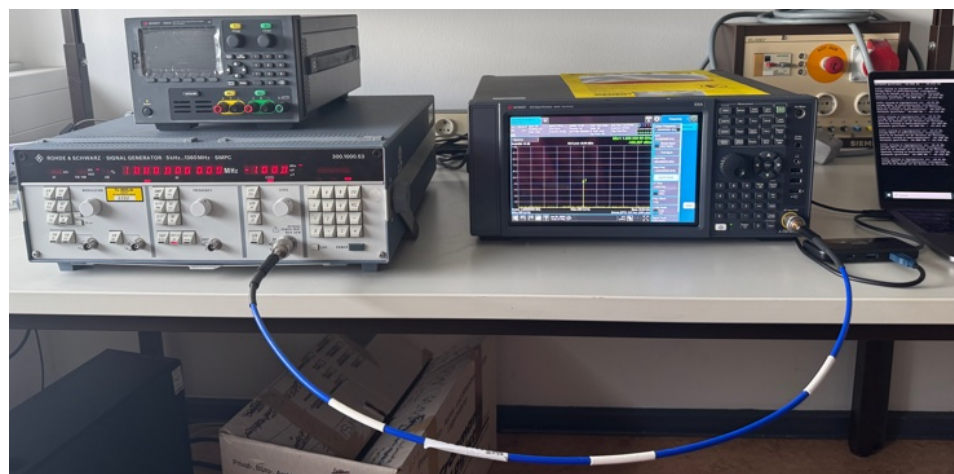


**Figure 12.1:** Calibration Signal Generator finished Setup



**Figure 12.2:** GPIB Connection to Signal Generator



**Figure 12.3:** Clock Synchronisation of Signal Generator



**Figure 12.4:** Dynamic Range Experiment Front Setup

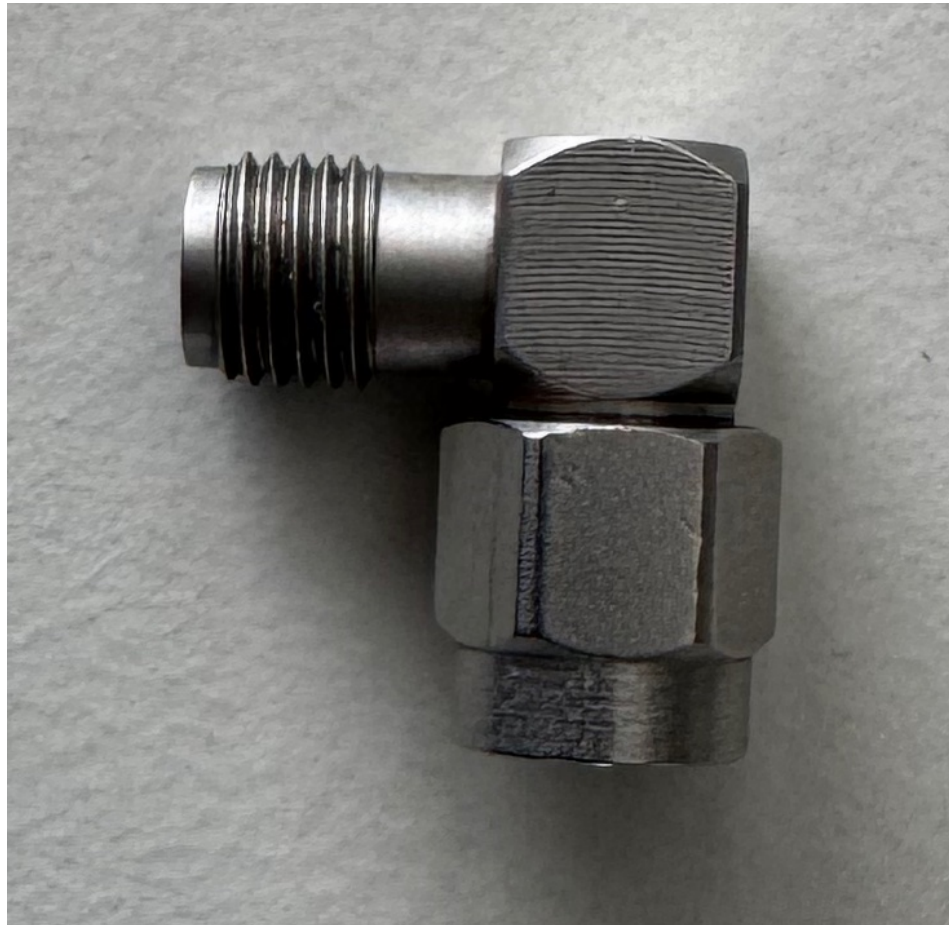


**Figure 12.5:** SMA Right Angle Adapter



**Figure 12.6:** Keysight EX36243A DC Source



**Figure 12.7:** Pluto SDR connected to Noise Source



**Figure 12.8:** Finished Setup to determine Noise Figure

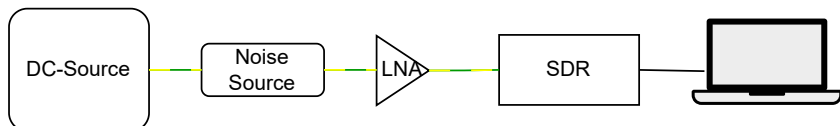


**Figure 12.9:** Noise Figure Measurement Sketch



**Figure 12.10:** Splitter



**Figure 12.11:** Splitter with Coaxial cable

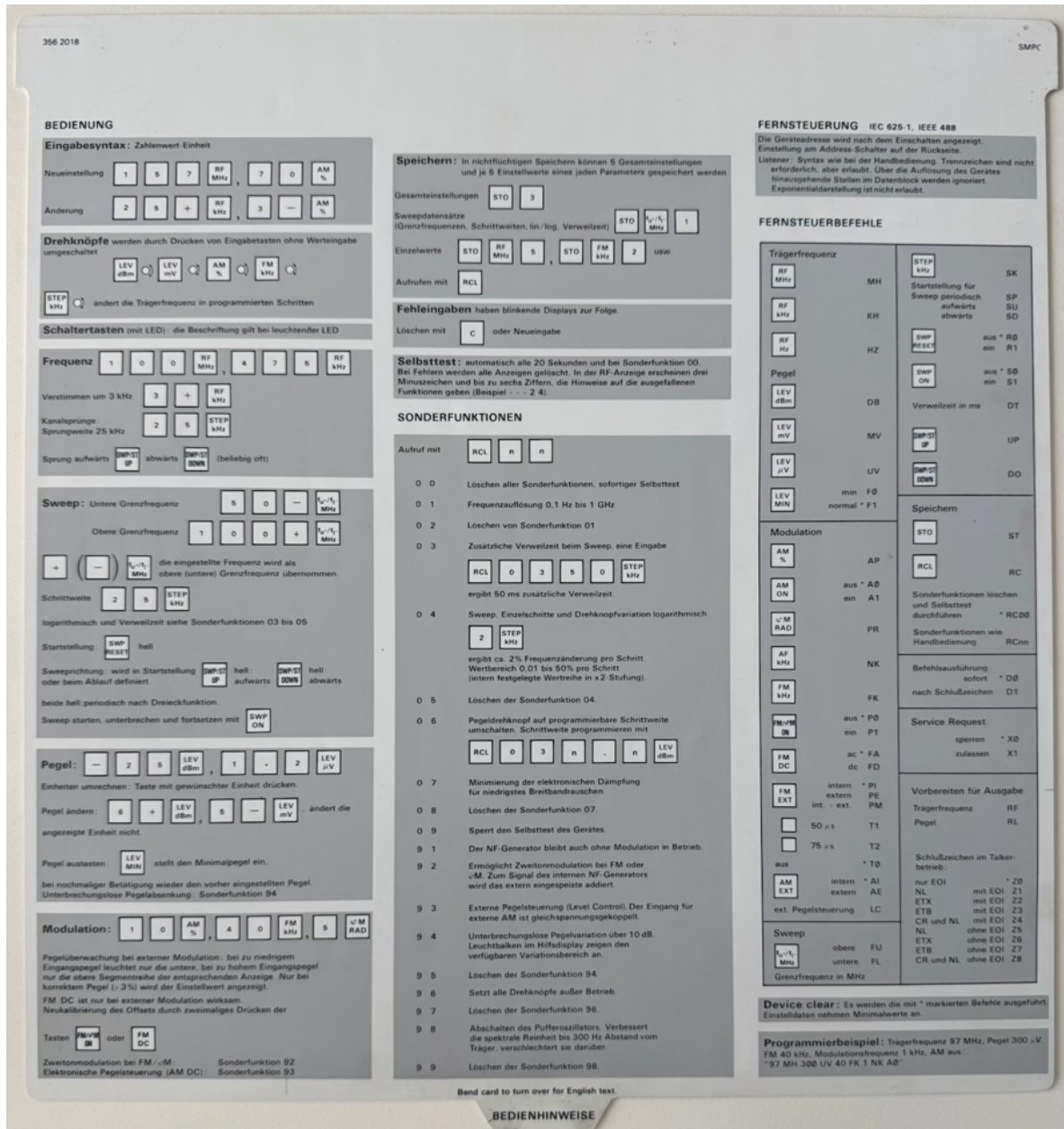


Figure 12.12: Manual and GPIB Commands for Signal Generator

## 12.2 Estimation of SDR Input Power

A reference value of an equivalent antenna noise temperature of  $T_A = 450$  K is assumed. This value is determined according to the measurement presented in [p.157, 16] (parabolic dish precisely aligned with the Sun). It is to note that, as explained in [p.147, 16], the measured equivalent antenna noise temperature is proportional to the square of the inverse half-power beamwidth. The latter quantity is smaller in our case due to the larger parabolic dish used. Furthermore, the measurement setup influences the atmospheric transmissivity, which also affects  $T_A$  ([p.157, 16]).

The output level of the LNB is calculated according to the relation in [p.147, (19), 16], where a noise figure of  $F_{LNB} = 0.5\text{dB}$  and a worst-case gain value of  $G_{LNB} = 50\text{dB}$  are taken from [13]. For simplicity, the antenna efficiency is set to  $\eta_A = 1$ <sup>1</sup>, so that  $T'_A = T_A$  can be assumed ([p.146 (11), 16]).

$$\begin{aligned} P_{\text{out, LNB}} &\approx (T_A + (F_{LNB} - 1) \cdot T_0) \cdot k_B \cdot B_{\text{SDR}} \cdot G_{\text{LNB}} \\ &\approx (450 \text{K} + (10^{\frac{0.5}{10}} - 1) \cdot 290 \text{K}) \cdot 1,38 \cdot 10^{-23} \frac{\text{J}}{\text{K}} \cdot 2 \cdot 10^6 \text{Hz} \cdot 10^{\frac{50}{10}} \\ &\approx -59 \text{dBm} \end{aligned} \quad (12.1)$$

---

<sup>1</sup>In practice, the efficiency is typically expected to lie between 60 % and 80 %. Since the resulting power is subsequently converted into dBm by applying the logarithm to calculate the expected power, the influence of the efficiency factor can be safely neglected for this approximation.

## 12.3 Dynamic Range Results

### 12.3.1 Dynamic Range Plots

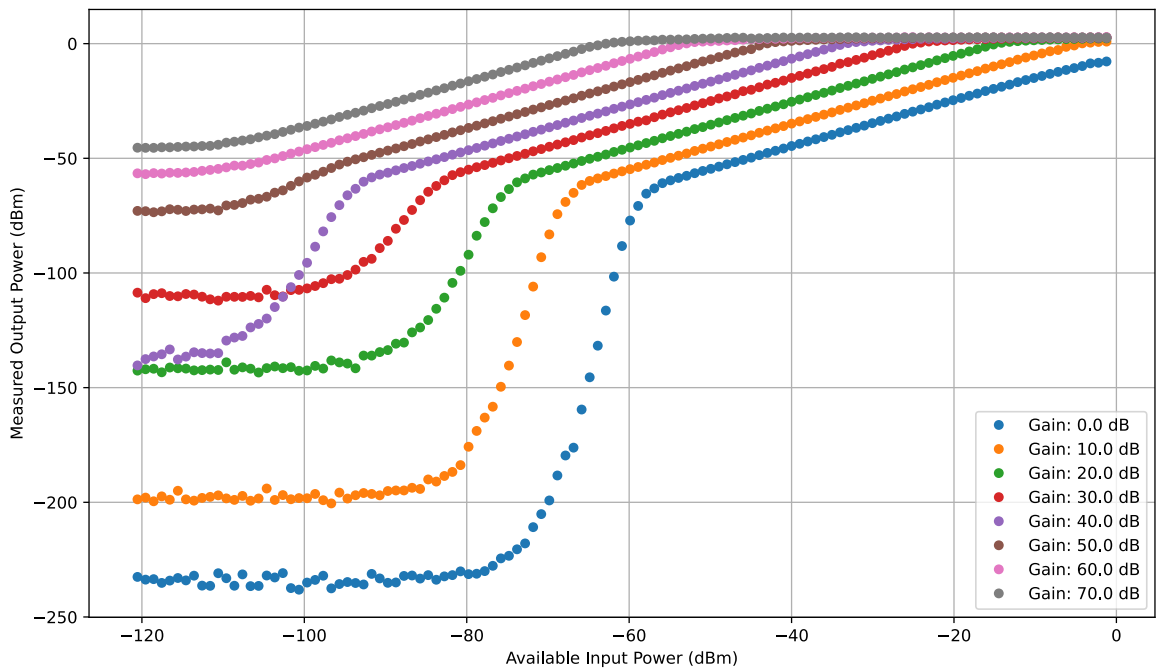


**Figure 12.13:** Results for the Dynamic Range of the Pluto SDR. Measured output power vs available input power for different gain settings.

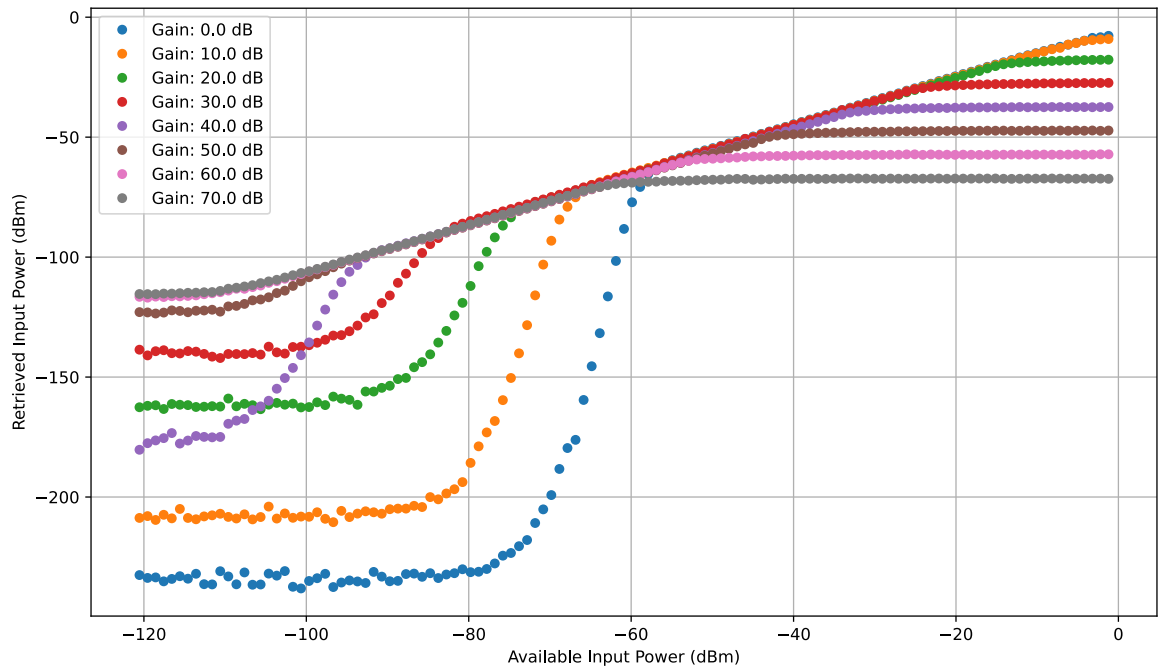


**Figure 12.14:** Results for the Dynamic Range of the Pluto SDR but it is shown the retrieved input power vs the available input power for different gain settings, meaning the gain was subtracted from the measured output power.

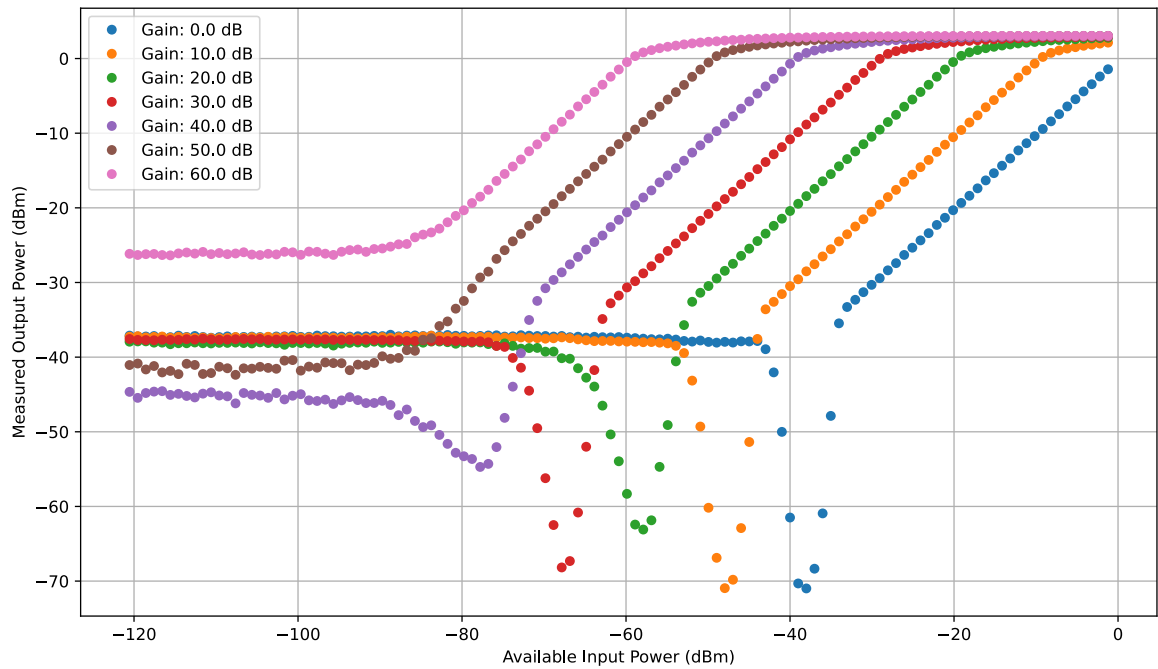


**Figure 12.15:** Results for the Dynamic Range of the HackRF SDR. Measured output power vs available input power.

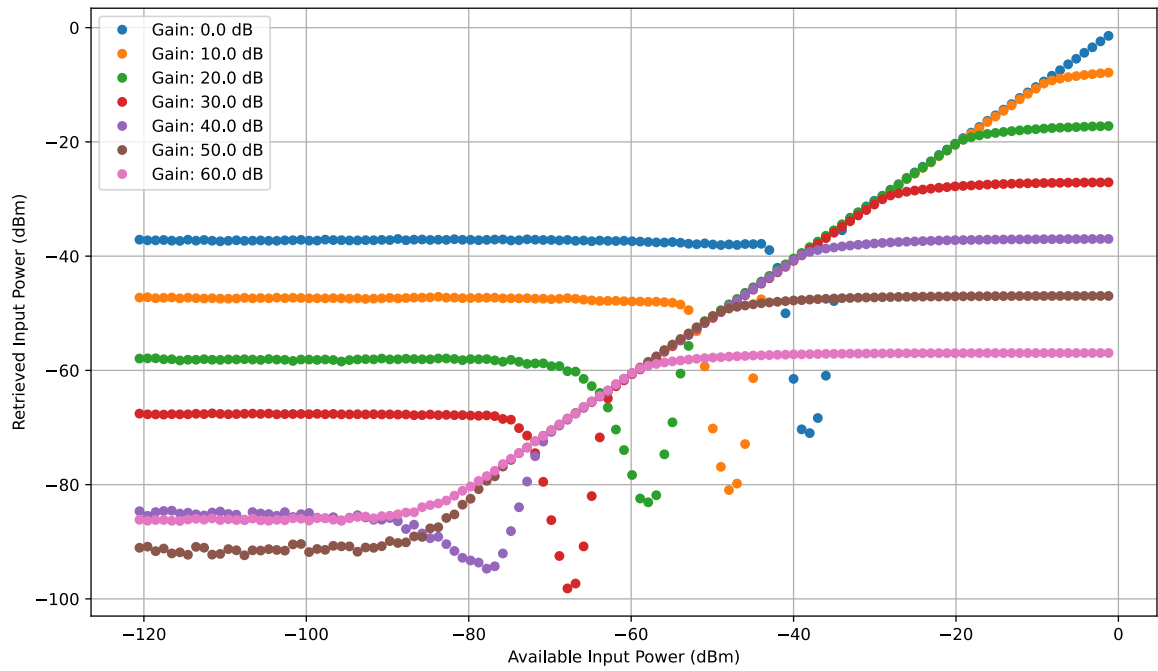


**Figure 12.16:** Results for the Dynamic Range of the HackRF SDR but it is shown the retrieved input power vs the available input power for different gain settings, meaning the gain was subtracted from the measured output power.

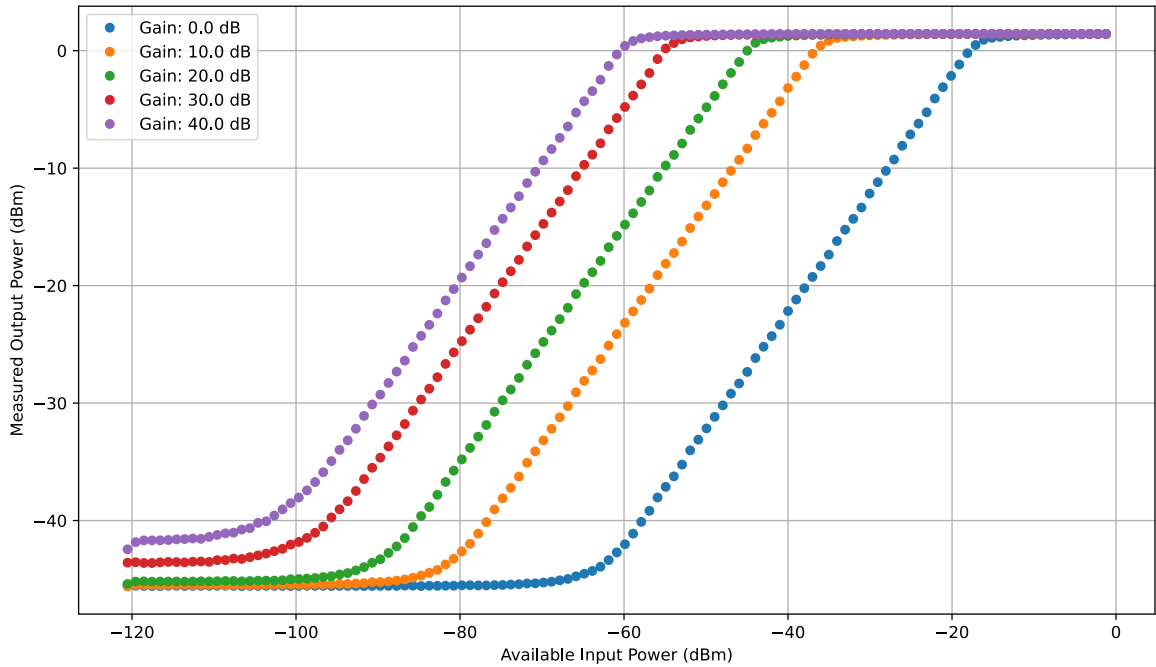


**Figure 12.17:** Results for the Dynamic Range of the RTL-SDR. Measured output power vs available input power.

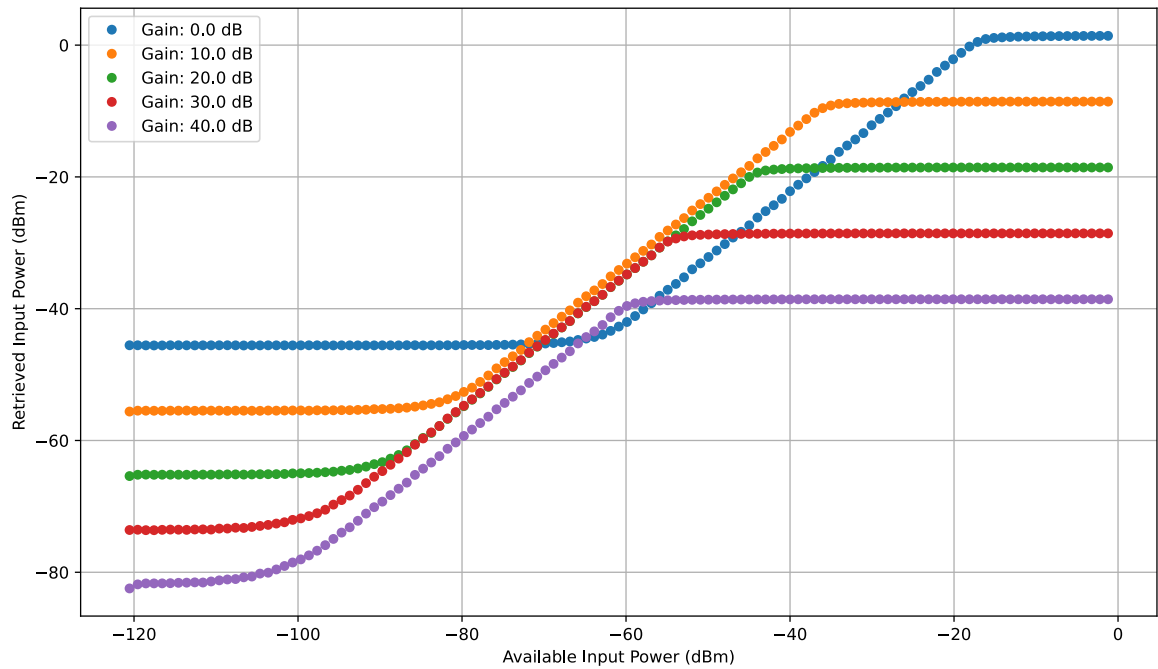


**Figure 12.18:** Results for the Dynamic Range of the RTL-SDR but it is shown the retrieved input power vs the available input power for different gain settings, meaning the gain was subtracted from the measured output power.

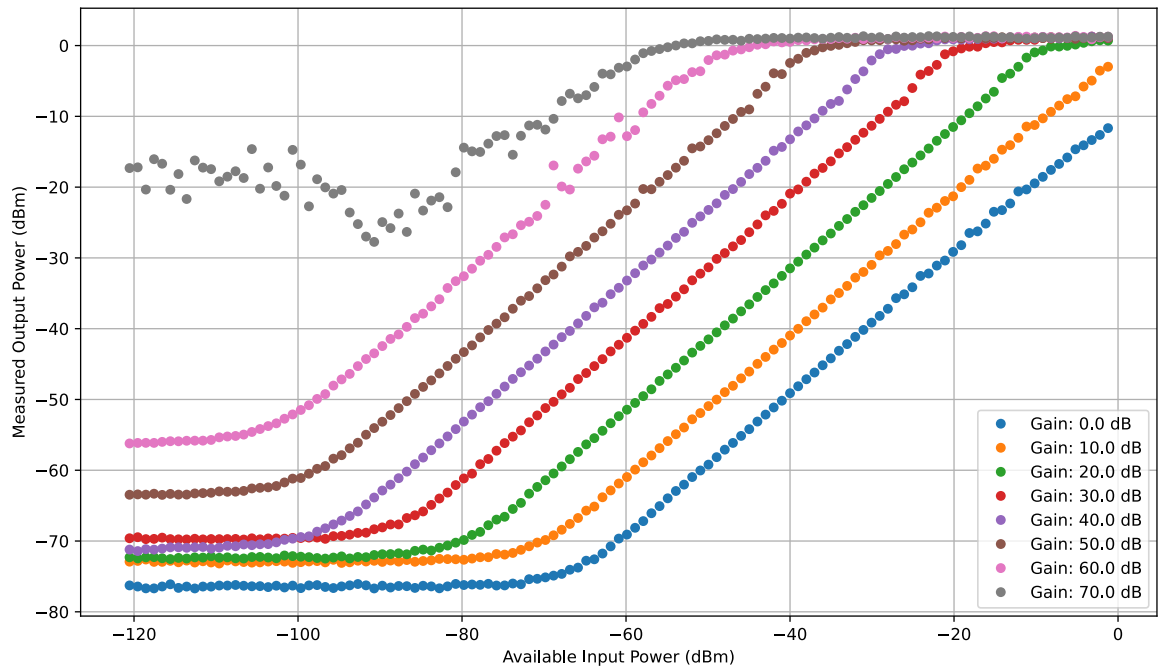


**Figure 12.19:** Results for the Dynamic Range of the USRP B200mini. Measured output power vs available input power.

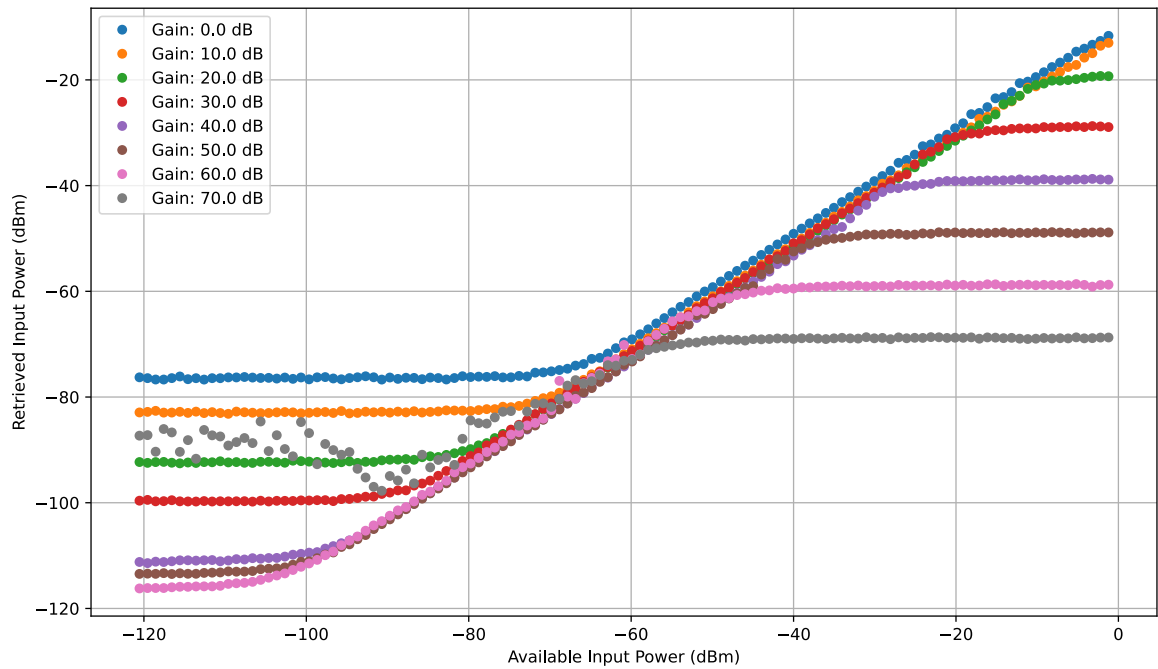


**Figure 12.20:** Results for the Dynamic Range of the USRP B200mini but it is shown the retrieved input power vs the available input power for different gain settings, meaning the gain was subtracted from the measured output power.

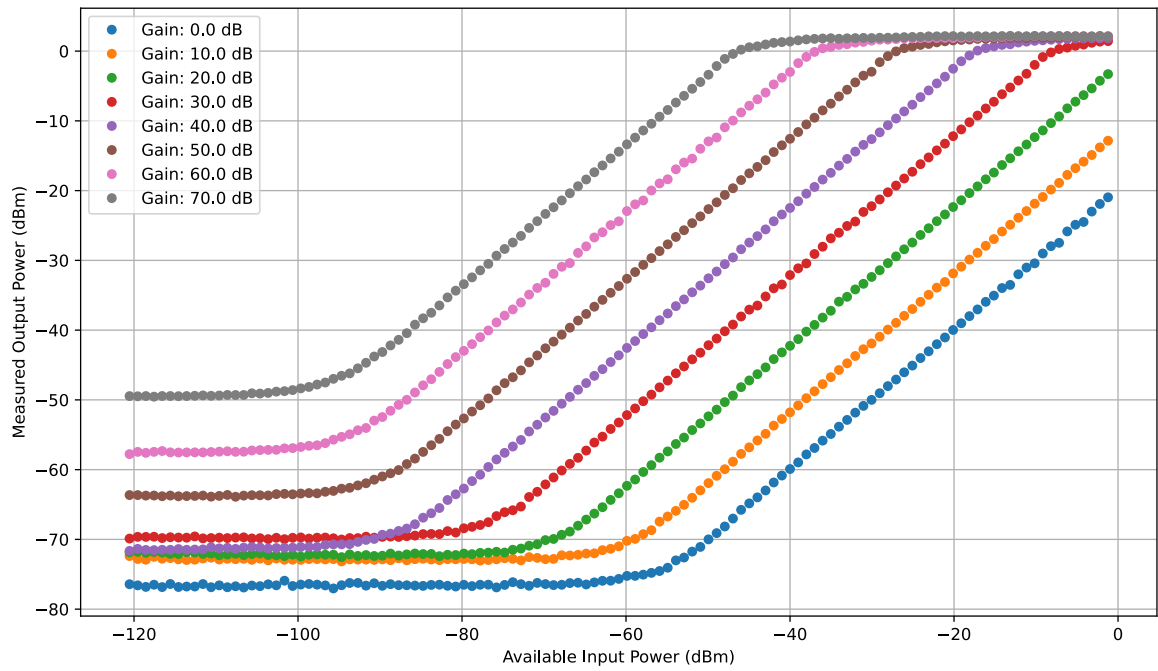


**Figure 12.21:** Results for the Dynamic Range of the USRP B210. Measured output power vs available input power.

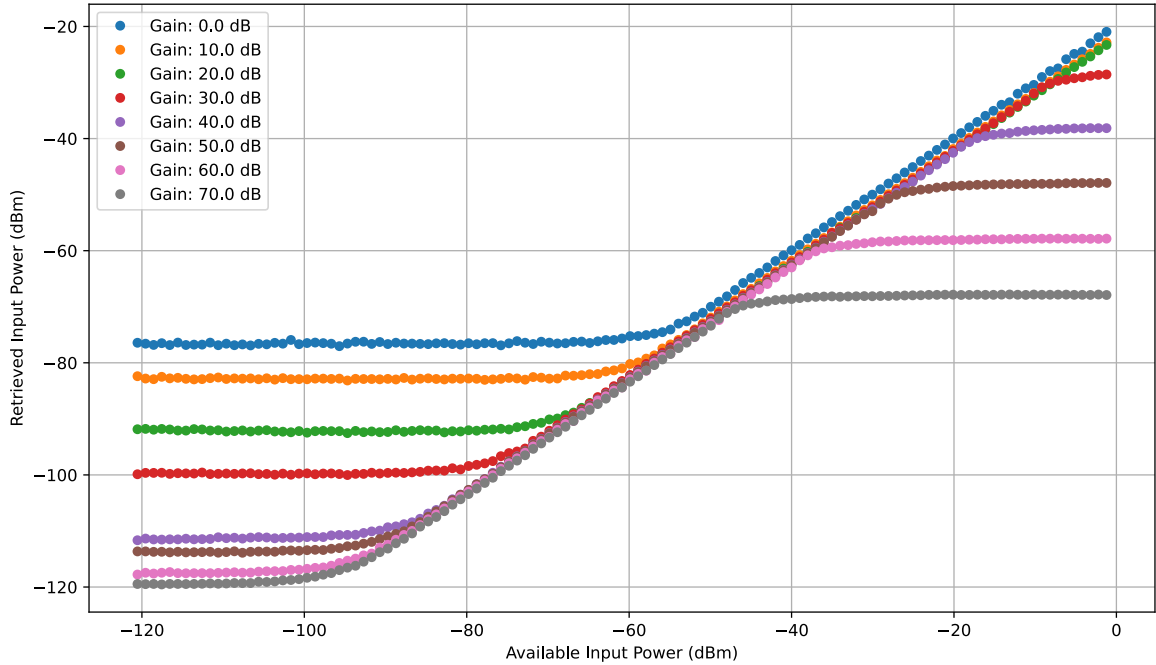


**Figure 12.22:** Results for the Dynamic Range of the USRP B210 but it is shown the retrieved input power vs the available input power for different gain settings, meaning the gain was subtracted from the measured output power.

### 12.3.2 Dynamic Range Tables

Gain	Input Power Range [dBm]	Offset	Offset - Gain	DR [dB]	ENOB
0.0	[-34,033; -1,219]	-0,132	-0,132	32,814	5,19
10.0	[-42,983; -7,185]	9,339	-0,661	35,798	5,66
20.0	[-51,932; -17,129]	19,327	-0,673	34,803	5,53
30.0	[-62,871; -27,073]	28,993	-1,007	35,798	5,66
40.0	[-70,826; -37,017]	39,052	-0,948	33,809	5,32
50.0	[-78,781; -48,949]	50,815	0,815	29,832	4,67
60.0	[-83,753; -57,899]	57,809	-2,191	25,854	4,00
70.0	[-82,759; -59,888]	59,878	-10,122	22,871	3,52

**Table 12.1:** Identified linear input power ranges and offset values for each gain setting of the HackRF SDR. These ranges define the effective dynamic range where the device maintains linear operation.

Gain	Input Power Range [dBm]	Offset	Offset - Gain	DR [dB]	ENOB
0.0	[-64,860; -16,134]	17,344	17,344	48,726	7,84
10.0	[-82,759; -34,033]	35,886	25,886	48,726	7,84
20.0	[-90,714; -41,989]	43,872	23,872	48,725	7,84
30.0	[-98,669; -52,927]	53,612	23,612	45,742	7,34
40.0	[-101,652; -58,893]	58,834	18,834	42,759	6,83

**Table 12.2:** Identified linear input power ranges and offset values for each gain setting of the RTL-SDR. These ranges define the effective dynamic range where the device maintains linear operation.

Gain	Input Power Range [dBm]	Offset	Offset - Gain	DR [dB]	ENOB
0.0	[-57,899; -1,219]	-20,150	-20,150	56,680	9,13
10.0	[-62,871; -1,219]	-11,983	-21,983	61,652	10,00
20.0	[-72,815; -1,219]	-2,496	-22,496	71,596	11,63
30.0	[-79,775; -4,202]	7,304	-22,696	75,573	12,34
40.0	[-90,714; -14,146]	16,833	-23,167	76,568	12,48
50.0	[-92,702; -24,090]	26,530	-23,470	68,612	11,14
60.0	[-94,691; -34,033]	36,046	-23,954	60,658	9,81
70.0	[-95,686; -43,977]	45,386	-24,614	51,709	8,32

**Table 12.3:** Identified linear input power ranges and offset values for each gain setting of the USRP B210. These ranges define the effective dynamic range where the device maintains linear operation.

Gain	Input Power Range [dBm]	Offset	Offset - Gain	DR [dB]	ENOB
0.0	[-68,837; -1,219]	-9,628	-9,628	67,618	10,91
10.0	[-74,803; -1,219]	-1,441	-11,441	73,584	11,88
20.0	[-82,759; -6,190]	8,184	-11,816	76,569	12,48
30.0	[-89,719; -16,134]	18,343	-11,657	73,585	11,88
40.0	[-99,663; -25,084]	26,257	-13,743	74,579	12,15
50.0	[-100,658; -35,028]	36,184	-13,816	65,630	10,63
60.0	[-99,663; -69,831]	45,866	-14,134	29,832	4,67

**Table 12.4:** Identified linear input power ranges and offset values for each gain setting of the USRP B200mini. These ranges define the effective dynamic range where the device maintains linear operation.

## 12.4 Gain Drift

### 12.4.1 Estimation of Receiver Sensitivity

We assume the unrealistic case that the LNB exhibits no gain drift, so  $\Delta G_{dB} = \Delta G_{dB,SDR}$ . The integration time for the estimation must correspond to the duration of the window in which the gain drift occurs. This allows us to assess the accuracy of the smallest detectable temperature change, assuming that this window length corresponds to a calibration interval. The noise figure of the receiver chain is assumed to be 0.5 dB (see eq. (8.2) for justification). The antenna temperature is taken from the measurement in [p.147, 16], as previously explained in section 12.2. Possible influencing factors, as already mentioned in section 12.2, should again be kept in mind.

$$\frac{\Delta G}{G_0} = \frac{10^{\frac{G_{t_0,dB}}{10}} - 10^{\frac{G_{t_1,dB}}{10}}}{10^{\frac{G_{t_0,dB}}{10}}} = 1 - 10^{\frac{G_{t_1,dB} - G_{t_0,dB}}{10}} = 1 - 10^{\frac{\Delta G_{dB}}{10}} \quad (12.2)$$

$$\Delta T_{min} = [450K + (10^{\frac{0.5}{10}} - 1) \cdot 290K] \cdot \sqrt{\left(\frac{1}{2 \cdot 10^6 Hz \cdot 15 \cdot 60s}\right)^2 + (1 - 10^{\frac{-0.43}{10}})^2} \approx 46K \quad (12.3)$$

$$\Delta T_{min} = [450K + (10^{\frac{0.5}{10}} - 1) \cdot 290K] \cdot \sqrt{\left(\frac{1}{2 \cdot 10^6 Hz \cdot 30 \cdot 60s}\right)^2 + (1 - 10^{\frac{+0.13}{10}})^2} \approx 15K \quad (12.4)$$

## 12.5 Integration Time

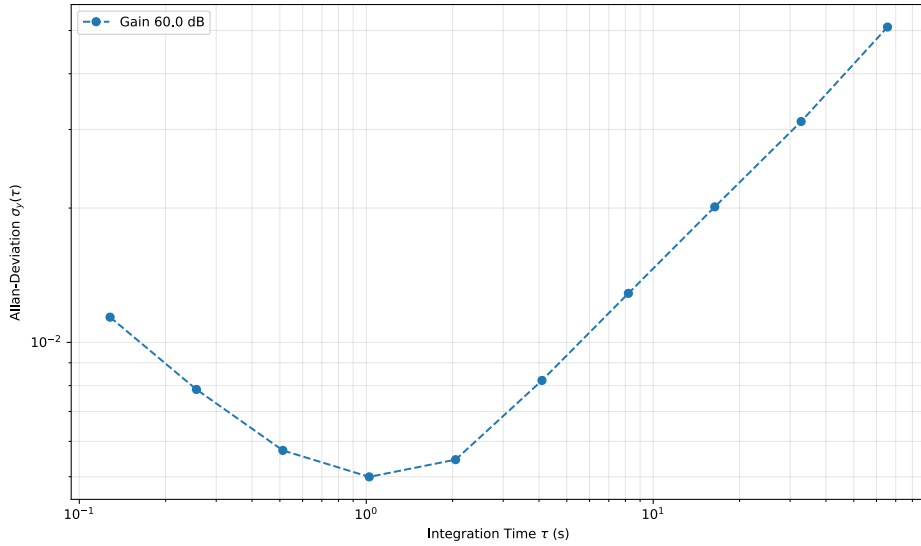


**Figure 12.23:** Allan Deviation for different integration time intervals for several gains of the HackRF SDR, first measurement set

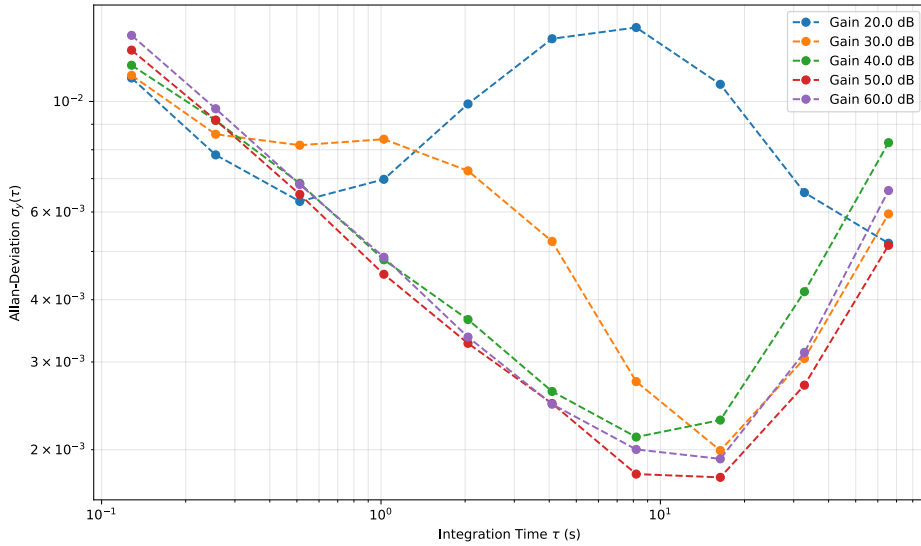


**Figure 12.24:** Allan Deviation for different integration time intervals for several gains of the USRP B200 mini, first measurement set

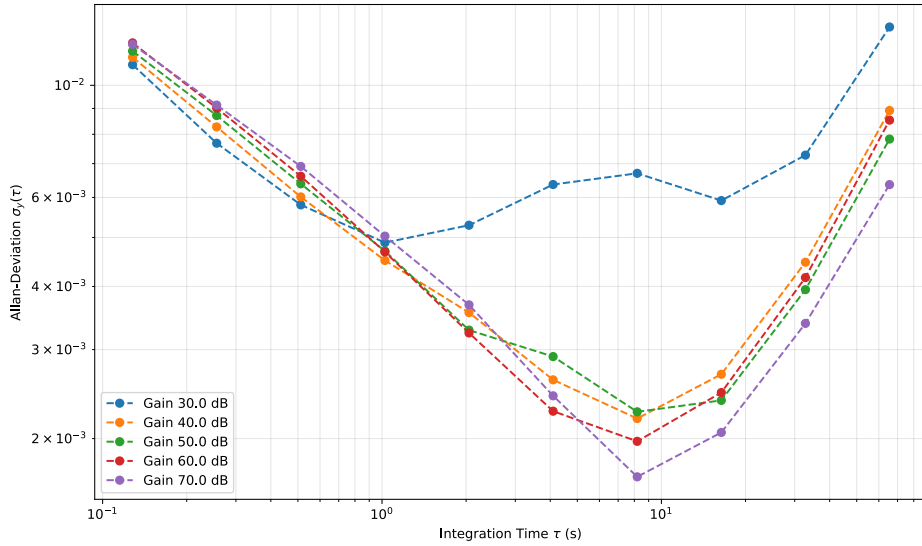


**Figure 12.25:** Allan Deviation for different integration time intervals for several gains of the Pluto SDR, second measurement set

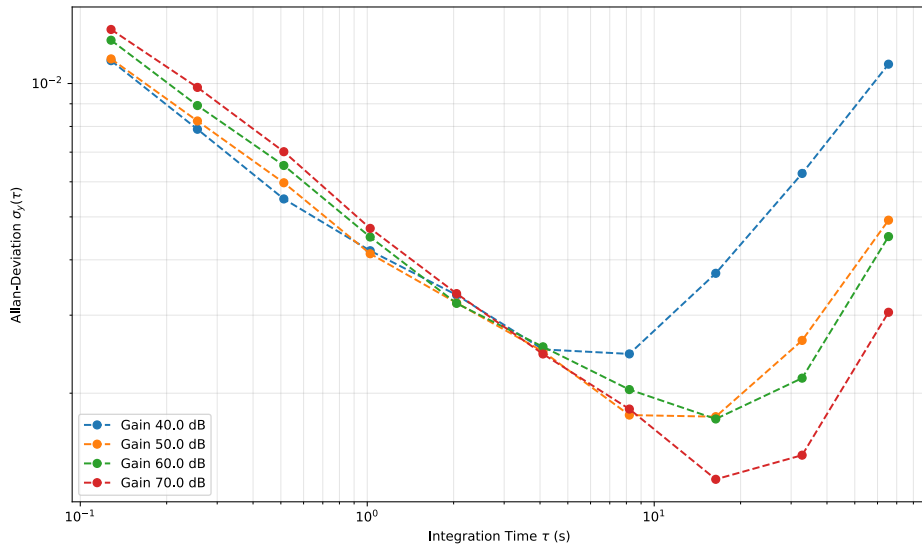


**Figure 12.26:** Allan Deviation for different integration time intervals for several gains of the USRP B210, second measurement set

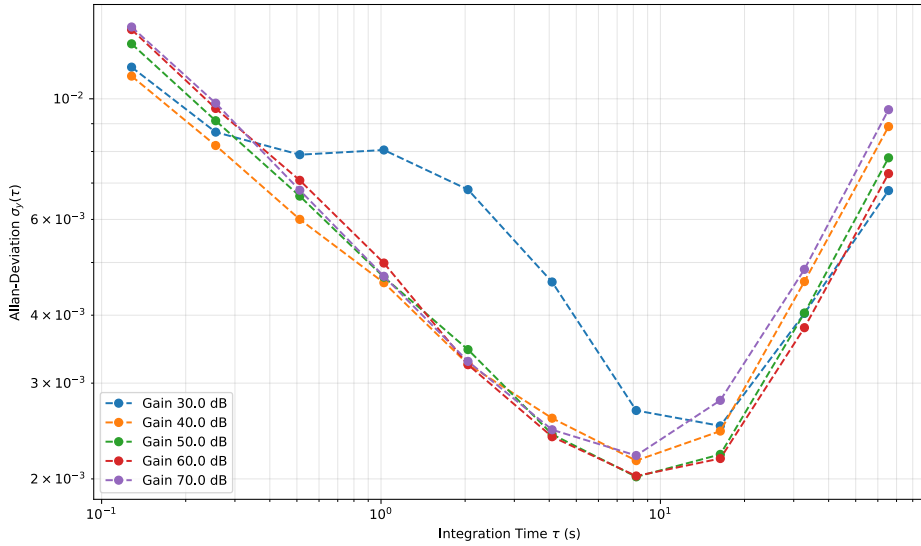


**Figure 12.27:** Allan Deviation for different integration time intervals for several gains of the USRP B200 mini, second measurement set

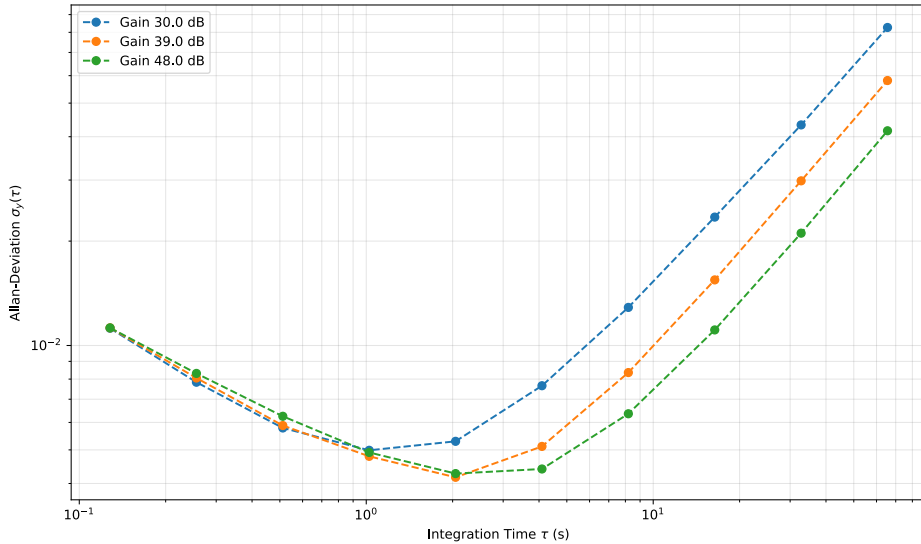


**Figure 12.28:** Allan Deviation for different integration time intervals for several gains of the RTL SDR, second measurement set

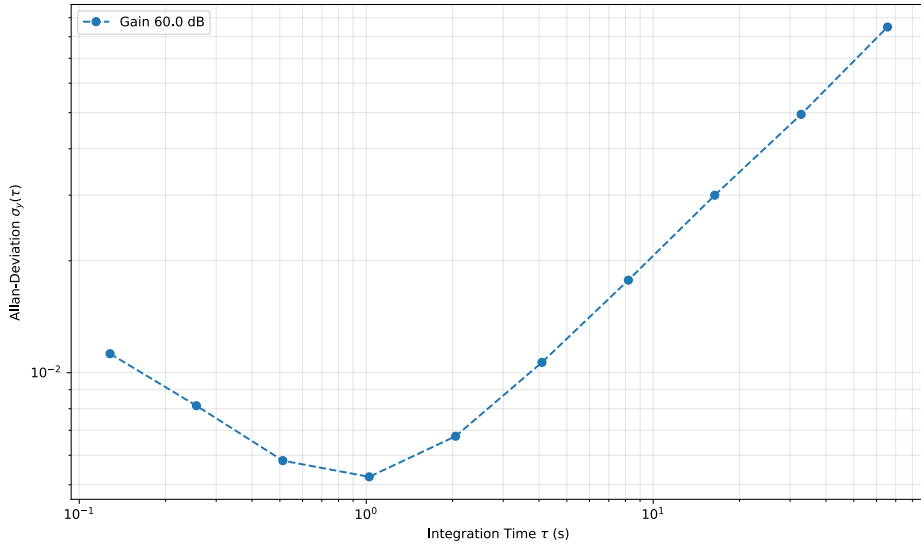


**Figure 12.29:** Allan Deviation for different integration time intervals for several gains of the Hack RF, second measurement set

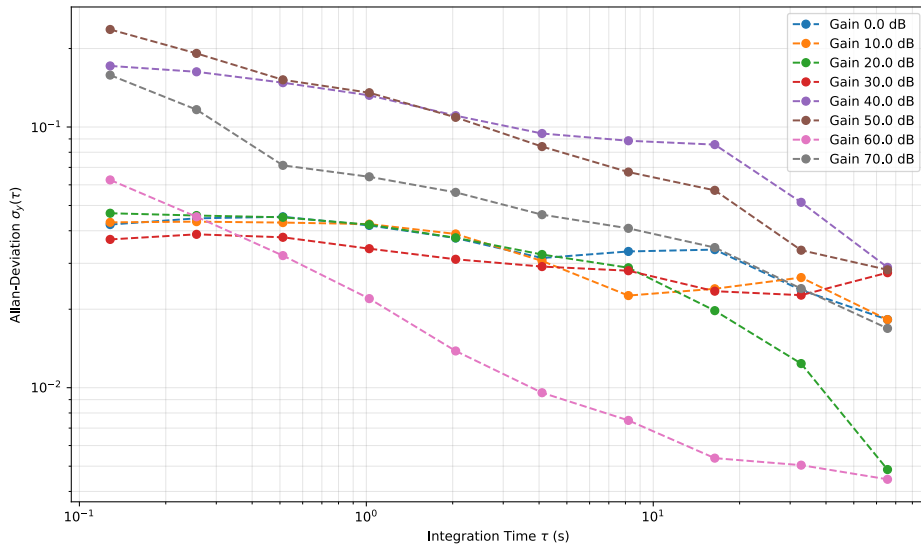


**Figure 12.30:** Allan Deviation for different integration time intervals for several gains of the HACKRF, wrong measurement setup, first measurement set

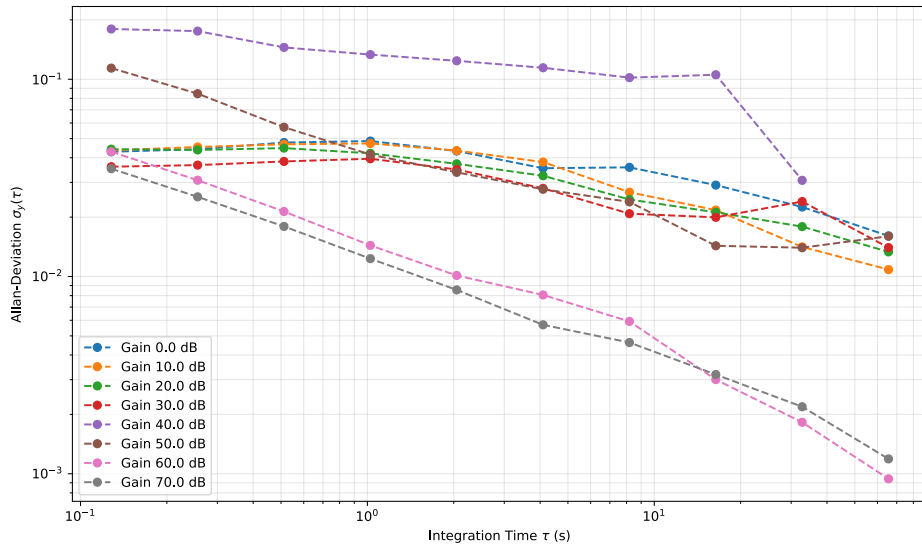


**Figure 12.31:** Allan Deviation for different integration time intervals for several gains of the HACKRF, wrong measurement setup, second measurement set

## 13 Affidavit of Independent Work and Declaration of AI Use

We, Daniel Schreiber and Leo Müller, hereby declare under oath that the submitted work, is our own independent work.

We have not used any sources or aids other than those explicitly stated in this work. All parts of the work that have been taken directly or indirectly from other sources have been identified and cited.

We explicitly declare that Artificial Intelligence (AI) tools were used for this work. The nature and extent of this usage are detailed as follows:

- translations of text from German to English
- formulations, grammar and spelling correction of the final text
- cleaning, generating and debugging python code for plotting and automation
- generating LaTeX code for formatting
- generation of the affidavit's preliminary wording
- compile and sort the abbreviations list



---

Daniel Schreiber



---

Leo Müller